Investigating the Role of Lysosomal Acid Lipase (LAL) in the Skeletal Niche

Scientific Research Paper

On behalf of the Austrian Marshall Plan Foundation Scholarship Program

By Alena Akhmetshina, MSc.

Research stay at Vanderbilt University Medical Center:

December 1st, 2022 – May 31st, 2023

Supervisor at the Medical University of Graz:

Univ.-Prof. Mag. Dr.rer.nat. Dagmar Kratky

Supervisor at the host institution (Vanderbilt University Medical Center/ Vanderbilt University):

Assistant Prof., Ph.D., Elizabeth Rendina-Ruedy

Abstract.

Lysosomal acid lipase deficiency (LAL-D) has been linked to an increased risk of fracture and impaired bone homeostasis through interaction with osteoblast metabolism. However, the complete mechanism has not been described yet in a cell-specific manner. Complementary to these studies, bone marrow adipose tissue (BM-AT) is a unique type of AT that represents more than 10% of total fat mass in lean and healthy people. Recently, it has been demonstrated that BM-AT has high expression of LAL, which, together with elevated cholesteryl ester (CE) concentrations in this tissue, suggests an important role of this enzyme in the metabolism of BM-AT. Therefore, the aims of this study were to understand the involvement of LAL in osteoblast development, bone production, and bone marrow-derived adipocyte (BM-Ad) metabolism to gain a deeper molecular understanding of the effects of dyslipidemia and cholesterol homeostasis on skeletal health.

For our first aim, osteoblast-specific Lal-deficient (bLal-/-) mice were generated in Dr. Rendina-Ruedy's laboratory by crossing Lipa$^{fl/fl}$ with OCN(*Bglap*)-Cre mice. The goal of the project was to characterize the skeletal and metabolic phenotype. Surprisingly, these mice showed no significant differences in the bone or in metabolic parameters compared to their littermate controls. Nevertheless, minor differences were observed in the bone microarchitecture of female bLal-/- mice. Since these mice did not show sufficient recombination and subsequent *Lipa* gene repression, many of these results remain questionable and inconclusive.

For our second aim, BM-Ad were treated with an inhibitor of LAL, Lalistat 2, to determine the role of LAL in adipogenesis. We observed that Lalistat 2 treatment increased *Plin2*, suggesting an increase in lipid droplets, and altered the bioenergetic status of BM-AT.

During my research stay, I published one review paper as the first author on the influence of cholesterol on the regulation of osteoblast function (doi: 10.3390/metabo13040578) and I was a co-author on a scientific publication "Altered osteoblast metabolism with aging results in lipid accumulation and oxidative stress mediated bone loss" (doi: 10.14336/AD.2023.0510).

Table of content

1. Introduction.

1.1 Cellular cholesterol homeostasis

Cholesterol is utilized by all tissues to maintain membrane permeability and fluidity. Additionally, it functions as a precursor for the production of compounds essential for the body, including vitamin D, bile acids, and steroid hormones (1). As a result, the regulation of cholesterol metabolism is quite strict. The two most well characterized processes for controlling cholesterol homeostasis are its biosynthesis pathway as well as cellular uptake of cholesterol-containing low-density lipoprotein (LDL) particles from the circulation executed by LDL receptor (LDLR)-mediated endocytosis (2).

Endogenous production of cholesterol from acetyl-CoA precursors in a multi-step process, starting with the formation of acetoacetyl-CoA from two molecules of acetyl-CoA, which is followed by the formation of β-hydroxy-methylglutaryl-CoA (HMG-CoA) from acetoacetyl-CoA and a third acetyl-CoA molecule by HMG-CoA synthase. Thereafter, this molecule is reduced in the rate-limiting step of the pathway to mevalonate by the enzyme HMG-CoA reductase (HMGCR) (3).

Alternatively, circulating lipoproteins are taken up by receptor binding and endocytosis, after which endosomes fuse with lysosomes and neutral lipids such as cholesteryl esters (CEs) and triglycerides (TGs) from the lipoprotein particles are degraded by lysosomal acid lipase (LAL) (4). While sterol regulatory element-binding protein (SREBP) and proprotein convertase subtilisin/ kexin type 9 (PCSK9) regulate intracellular cholesterol through modulation of cholesterol synthesis or LDLR expression and membrane LDLR abundance, respectively, LAL activity is essential for the cytosolic release and cellular availability of free cholesterol originating from extracellular sources. Recent studies have shown a physiological link between lysosomal lipid breakdown and autophagy (5).

1.2 Importance of cholesterol homeostasis in osteoblasts

Publications from the last 3 decades demonstrated the significance of cholesterol in the process and metabolism of bone growth. Niemeier et al.'s study discovered a substantial role for bones in lipoprotein catabolism. By using radioactively labeled chylomicron remnants (CR), the authors were able to demonstrate that the liver and bones compete and even equally contribute to the removal of CR *in vivo* (6). Thereafter, it was established that cholesterol and its metabolic intermediates are necessary for the maturation of MSCM2-10B4 mouse marrow stromal cells (MSCs), as osteoblastic differentiation of pluripotent

MSCs was suppressed by the inhibition of cellular cholesterol biosynthesis through HMGCR (7). Additionally, treatment of murine mesenchymal stem cells with cholesterol resulted in cellular proliferation and the production of mineralized nodules, as evidenced by an increase in alkaline phosphatase (ALP) activity along with expression of other key osteoblast differentiation genes (8). Elevated cholesterol concentrations suppressed the proliferation and differentiation rates of MC3T3-E1 osteoblasts, while also increasing oxidative damage (9). Reduced proliferation of the bone marrow stroma osteogenic cell population through reducing ALP activity, collagen processing, and mineralization was also noticed upon treatment of these cells with minimally oxidized low-density lipoprotein (MM-LDL), likely through PPAR and mitogen-activated protein kinase-dependent pathway (10). Although alterations in cholesterol homeostasis affect osteoblast function, it appears that its impact on either osteoblast or bones in general depend on both dose and exposure time.

Experiments in rodents fed a high cholesterol diet confirmed these *in vitro* findings as mice provided a hypercholesterolemic diet developed osteoporosis or low bone mass (11–13), whereas a high-cholesterol feeding in rats triggered hypercholesterolemia-increased bone resorption and -decreased bone formation, resulting in lower bone mineral density (BMD) (9).

Lipoproteins have been found to play a role in a variety of bone disorders. Recent publications postulated that osteoblasts that are unable to obtain cholesterol via LDL, such as those found in Ldlr-/- mice, exhibit lower ALP activity, defective mineralization, and consequently impaired osteoblastogenesis (14).

Human data have shown a link between circulating cholesterol and bone health, with the majority of studies reporting an inverse relationship between LDL-C and BMD. Patients with hypercholesterolemia, for example, had a higher bone turnover, which was correlated to total and LDL-cholesterol (15,16). Moreover, in the study participants with the mutated apolipoprotein B-100 a deleterious bone phenotype was detected (17). Of note, the administration of statins (commonly prescribed medications used to lower cholesterol via inhibition of HMGCR) both *in vivo* (18) and *in vitro* (8,9,19–22) stimulated osteoblast activity, which in turn increased bone production. However, it is yet unknown whether this is a result of decreased circulating LDL levels or because of statins' anti-inflammatory properties.

Taken together, these findings imply that potentiated cholesterol biosynthesis may have a deleterious effect on osteoblasts, although the underlying molecular mechanism remains obscure.

1.3 Essential role of LAL in lipid metabolism

The role of LAL in lipid metabolism has been evidenced in mice and humans affected by LAL deficiency (LAL-D), an autosomally-recessive inherited metabolic disease (frequency between 1:40,000 to 1:300,000 depending on the population), in which LAL gene mutations lead to defective or non-functional enzymatic activity of LAL. This ultimately results in defective lipid metabolism with ectopic CE and TG accumulation and organ damage (23).

Historically, there are two clinical forms of LAL-D. In 1956, the first case of severe emaciation, hepatosplenomegaly, and adrenal calcification followed by death in the first month of life was described (24) and the condition was named Wolman's disease (WD). The enzyme activity in these patients is less than 1% of the normal activity. Pathological accumulation of neutral lipids in the spleen, adrenal glands, lymph nodes, mucosa of the small intestine, vascular bed, and skeletal muscles (SMs) determine the nature of the pathology. The clinical manifestations of WD are persistent vomiting, diarrhea, steatorrhea, and occasional jaundice. Hepatic fibrosis and cirrhosis develop rapidly, following massive accumulation of CEs and TGs (25). Fatal outcome occurs against the background of rapidly progressing multiple organ failure at the age of 6-12 months (26).

The second, milder form of LAL-D is cholesterol esterase storage disease (CESD) firstly described in 1963 (27). This form of LAL-D is characterized by a later onset of clinical manifestations and slow progression. Enzyme activity of LAL in this form of the disease is 1-12% of normal. The age of onset varies widely from 2 to 25 years of age. The main symptom is hepatomegaly found in the majority of patients. An early biochemical marker of liver damage - cytolysis syndrome - is manifested by elevated serum levels of aspartate aminotransferase and alanine aminotransferase (26). Although CESD is rare, it is likely that many patients are unrecognized or misdiagnosed.

Opposite to humans, LAL-deficient (Lal-/-) mice are viable, with a median lifespan of almost one year. They also exhibit ectopic TG and CE accumulation (particularly affecting liver, spleen, mesenteric lymph nodes, and small intestine), along with growth retardation, complete loss of white and partial loss of brown adipose tissue due to abnormal lipid metabolism (28–32). Unexpectedly, Lal-/- mice are a phenotypic model for CESD, but a biochemical and histopathological model for WD.

1.4 LAL impacts osteoblastogenesis and possibly affect bone marrow adipocytes

Prof. Rendina-Ruedy's team previously demonstrated that Lal-/- mice of both sexes exhibit lower trabecular bone volume relative to total volume (BV/TV; %) of the distal femur

metaphysis as well as thinner cortices of the femoral mid-diaphysis compared to wildtype (WT) controls. Lal-/- mice have considerably decreased osteoblast numbers (N.Ob) relative to total area (T.Ar). Despite the significant ectopic lipid accumulation associated with LAL-D, Lal-/- animals, however, do not exhibit enhanced bone marrow adiposity (33). Moreover, Lal gene (*Lipa* Cq 24, 10 ng cDNA) and protein are largely expressed in primary bone marrow stromal cells (BMSCs) during osteoblast differentiation and in the femur cortex (without bone marrow). Osteoblast development (as measured by ALP staining) is attenuated in calvaria osteoblasts (cOB) and BMSCs treated with the LAL inhibitor Lalistat 2 (33). Finally, and most importantly, lipidomic data demonstrates that LAL inhibition increases CE in osteoblasts, both immature stromal cells (day 0) and mature matrix secreting cells (day 7), which presumably decreases free cholesterol availability and affects its signaling (33). Thus, Prof. Rendina-Ruedy and colleagues discovered that Lal-/- mice have a reduced bone mass and fewer osteoblasts.

Compelling clinical data presented in the paper additionally demonstrate that individuals suffering from LAL-D display a skeletal phenotype that translates to an increase in fracture incidence irrespective of their age, sex and race (33). However, the mechanism underlying the impaired bone homeostasis in LAL-D is still not clear.

Recent data additionally have confirmed a link between increased bone marrow adipocyte (BM-Ad) numbers and aging, obesity, and osteoporosis, suggesting a role of these cells in bone structure and metabolism, thus influencing systemic homeostasis (34–38). The expression of LAL in BM-Ad cells is quite high, but the exact role of LAL in BM-AT remains unexplored (34). Interestingly, BM-Ads have a unique lipid metabolism since they lack classical lipid droplets degradation machinery mediated by adipose triglyceride lipase, but rather exhibit a cholesterol-orientated metabolism. Thus, BM-Ads could be an important source or a buffering tissue for cholesterol and related metabolites. Therefore, studies are required to examine how cholesterol pathways can affect skeletal metabolism and whether LAL is involved in cholesterol homeostasis in BM-Ads.

1.5 Cholesterol metabolism via LAL supports osteoblast bioenergetic capacity

Given our results showing that inhibiting LAL enhances CE accumulation in osteoblasts, a reduction in intracellular free cholesterol derived through the LDL-LDLR-LAL route is indicative, suggesting a possible shift of cholesterol metabolism toward the biosynthetic pathway. It is also worth mentioning that cholesterol biosynthesis is a complex process that requires 18 moles of acetyl-CoA, 36 moles of ATP (according to some sources even 99

molecules of ATP (39)), 16 moles of NADPH, and high oxygen consumption to yield 1 mole of cholesterol. In addition, acetyl-CoA carboxylase and HMGCR activities reflect not only the cellular demand for cholesterol and fatty acids but also the availability of common substrates (particularly citrate and acetyl-CoA) (40). The availability and demand of these common precursors depend on the metabolic activity of the cell as a whole, which may have an impact on the cellular energy status.

Our previous data suggest that cholesterol generation via the biosynthetic pathway exerts a negative impact on osteoblasts. While these data are somewhat counterintuitive, ATP that was originally destined to support bone formation is now presumably redirected to generate cholesterol, thereby impairing bone formation. In line, providing cholesterol via the LDL-LDLR-LAL pathway would be preferred during active bone formation as means to spare ATP.

While previous investigation has shown that Lal-/- mice have low bone mass and that LAL inhibition impairs osteoblastogenesis and alters lipid metabolism, conditional genetic deletion of *Lipa* (gene encoded LAL) in osteoblasts directly is required to investigate *in vivo* mechanisms regulating bone formation through osteoblast function. The possible systemic consequences of global LAL deficiency, including fat malabsorption, vitamin and mineral deficiencies, systemic inflammation, lipodystrophy, and insulin resistance, may interfere with bone homeostasis, thereby indirectly leading to the skeletal phenotype observed in Lal-/- mice. Based on our compelling *in vitro* evidence suggesting that LAL also works in a cell-autonomous manner in the osteoblast, we conclude that the most appropriate model to fully examine the skeletal phenotype is osteoblast-specific LAL (*Lipa*) knock-out mouse model.

To better understand lipid metabolism of BM-Ad, osteoblasts, and bone in general and determine whether it depends on the presence of LAL, we aimed to perform the following experiments with the support of Dr. Rendina-Ruedy's laboratory at Vanderbilt University Medical Center:

(i) Characterizing bone-specific Lal-/- (bLal-/-) mice including metabolic and skeletal phenotyping;

(ii) Initial analyses of the role of LAL in BM-Ad.

2. Material and Methods

Mice

Experiments were performed using male and female age- and sex-matched control (Lipa $^{fl/fl}$ OCN-Cre -/-) and bLal-/- (Lipa $^{fl/fl}$ OCN-Cre +/+) mice. For BM-Ads, 7-8-week-old male and female C57BL/6J mice were purchased from Jackson Laboratory. Mice were maintained in a clean environment in accordance with guidelines of the Institutional Animal Care and Use Committee (IACUC). During maintenance, the mice were kept under standard 12 hours light/dark cycles and had ad libitum access to standard chow diet and water.

Genotyping

At the age of four to five weeks, animals were weaned. Toes were collected from 3-6 days old pubs and sent to Transnetyx, Inc. (Cordova, TN) for genotyping. I performed additional genotyping by digesting a piece of it in 75 µl lysis buffer (25 mM NaOH) at 95º C for 60 min and vortexing every 10-20 min. Afterwards, we added 75 µl of neutralization buffer (40 mM Tris HCl) to the sample tubes. The reaction mix contained 2 µl from each DNA sample, GoTaq green MM (Promega, Walldorf, Germany), 0.75 µM of each primer, and H_2O. For OCN-Cre genotyping forward: CAAATAGCCCTGGCAGATTC, reverse: TGATACAAGGACATCTTCC, for internal control (IC) (forward: CTAGGCCACAGAATTGAAAGATCT, IC reverse: GTAGGTGGAAATTCTAGCATCATCC primers were used. The following cycle conditions (program GoTaq28)**,** shown in Table 1, were used for the amplification of the specific DNA products.

Table 1. PCR program for OCN-Cre genotyping

Program Name	**PCR step**	**GoTaq28**
Polymerase/ Enzyme		GoTaq
Cycles		28
Cycle 1	Pre-denaturation	95º for 2 min
Cycle 2	Denaturation	95º for 30 s
Cycle 3	Annealing	58º for 30 s
Cycle 4	Extension	72º for 30 s
Cycle 5		Go to 2; 27 times

Cycle 6	Final Extension	
Cycle 7		4º forever

LAL fluorescent activity assay

I estimated LAL activity using the fluorogenic substrate 4-methyl-umbelliferyl-palmitate (4-MUP) as describe previously (30) with some modifications for bones. Briefly, flushed long bones (femurs) were homogenized using SPEX 6775 Freezer/Mill Cryogenic Grinder (Spex SamplePrep, Metuchen, NJ) and the received powder was dissolved in lysis buffer. Protein concentrations were quantified by Bradford assay. To prepare each sample, 200 µl of 4-MUP (10 mM) and 200 µl of phosphatidylcholine (16 mM) were combined in hexane, evaporated under a nitrogen stream, and then resuspended in 5 ml of sodium taurocholate (2.4 mM) by sonication. The samples were incubated for 30 minutes at 37°C with 50 µl of 4-MUP substrate, 125 µl of assay buffer (200 mM sodium acetate, pH 4.5), and 25 µl of cell lysate. The addition of 100 µl of 0.75 M Tris (pH 11) stopped the process. Relative fluorescence units (RFU) were determined at 360 nm excitation/460 nm emission on a Varioskan Lux (Thermo Scientific, Waltham, MA) using series of 4-MU dilutions as standard. Samples with addition of Lalistat 2 (30 µM) were used as extra control. LAL activity was expressed as nmol MU/mg protein.

Body weights

Body weights were measured on a standard balance in grams postmortem.

Dual energy x-ray absorptiometry (DXA)

I performed dual-energy X-ray absorptiometry (DXA) Faxitron UltraFocus (Faxitron Biooptics, Tucson, AZ) on control and bLal-/- mice 8,12, and 16 weeks after birth as previously described (41). The instrument was calibrated for offset images, dark images, and flat-field images before the measurement by a method provided by the manufacturer. The mineral content of hydroxyapatite reference material with known density and bone mineral content measured by DXA are closely associated ($r^2 = 0.997$).

Micro-computed Tomography (µCT)

Tibia from the mice were obtained by removing soft-adhering tissue and then preserved for 48 hours in 10% neutral-buffered formalin (NBF), followed by storage in 70% ethanol. I canned the proximal and mid-diaphysis of these tibiae using an ex vivo micro-computed

tomography (CT) scanner (Scanco50 Medical AG, Brüttisellen, Switzerland). For the tibia metaphysis and diaphysis (200 slices each), image stacks with an isotropic voxel size of 6 m were obtained using a peak X-ray tube intensity and current of 70 kVp and 114 mA, 500 projections per full rotation of the sample, and an integration time of 300 ms. An area of interest (ROI) 180 µm distal from the proximal tibia development plate, encompassing a region of secondary spongiosa extending distally by 1.2 mm, was selected for trabecular bone analysis. The 1.2 mm of cortical bone that ended at the tibia-fibular junction was examined.

Lipid isolation from bone and TLC analysis

The Bligh and Dyer procedure (42) was used to pulverize and extract total lipid from flushed tibia cortex (devoid of marrow materials). However, the powder made from the entire by crushing bone using Freezer/Mill Cryogenic Grinder flushed tibia after pulverization was weighed before being normalized using a chloroform:methanol (1:2) mix. To achieve a stronger and more thorough extraction, the powder was also left overnight in a chloroform/methanol mixture in a water bath at 37°C. The dried lipid extract was then placed onto TLC plates (Sigma, St. Louis, MO) after being resuspended in an equal amount of chloroform:methanol (2:1) (80 µl). Using the solvent system of hexane:diethyl ether:acetic acid (70:30:1), lipids were separated by developing the TLC plate at 4°C (Sigma, St. Louis, MO). To visualize the lipids, the TLCs were charred at 120°C after being dyed with 10% (wt/vol) copper sulphate in an 8% (vol/vol) phosphoric acid solution. I used Fiji to normalize and analyze the integrated density of the lipid bands from each sample to the weight of the powdered bone sample.

RNA isolation and qPCR

Total RNA from flushed femurs (femurs with removed bone marrow) or cells was isolated using Trizol reagent (Ambion, Austin, TX) according to the manufacturer's protocol. Briefly, bone powder received using Freezer/Mill Cryogenic Grinder or from scraped cell suspensions were dissolved in 500 µl of Trizol, vortexed vigorously, and stored overnight at -80°C. One hundred µl of chloroform were added per 500 µl Trizolt reagent, vortexed, and centrifuged at 8,500 rpm at 4°C for 15 min. The supernatant was transferred to a fresh tube, mixed with 500 µl of isopropanol, vortexed, and centrifuged at 8,500 rpm at 4°C for 10 min. Thereafter, the supernatant was discarded, pellets were washed twice with 75% ethanol and centrifuged again at 8,500 rpm at 4°C for 5 min. The supernatant was discarded, pellets

were air-dried and resuspended in 15-50 µl DEPC water. RNA concentrations were measured at 260 nm using Nanodrop one (Thermo Scientific, Waltham, MA). One µl RNA was used for concentration determination.

cDNA was prepared from RNA by reverse transcription. One or two µg RNA in 10 µl (adjusted with nuclease-free ddH_2O) were reverse transcribed by using the High-Capacity DNA Reverse Transcription kit (4374967, Thermo Scientific, Waltham, MA). cDNA was diluted 1:50 in nuclease-free ddH_2O if 2 µg or 1:25 if 1 µg of RNA was used for reverse transcription. Three µl of diluted cDNA, 0.5 µl of forward and reverse primer (stock solution, 100 µM, diluted 1:10 with nuclease-free ddH_2O), and 5 µl PowerUP SYBR Green (A25742, Thermo Scientific, Waltham, MA)) were pipetted into a MicroAmp Optical 384 Well Reaction plate (Applied biosystems*,* San Francisco, CA*) to* do gene analysis on a QuantStudio 5 (Thermo Scientific, Waltham, MA). Samples were analyzed in duplicate and normalized to the expression of *cyclophilin A* as reference genes. Expression profiles and associated statistical parameters were determined using the $2^{-\Delta\Delta CT}$ method. Primer pairs are shown in Table 2.

Table 2. Primers used for real-time PCR

Gene	Forward primer	Reverse primer
Lipa	GCTGGCTTTGATGTGTGGATG	ATGGTGCAGCCTTGAGAATGA
Cyclophilin A	CCATCCAGCCATTCAGTCTT	TTCCAGGATTCATGTGCCAG
Sp7	GAAGTTCACCTGCCTGCTCTG	CGTGGGTGCGCTGATGT
Alpl	GGTATGGGCGGCGTCTCCACA	GCCCGTGTTGTGGTGTAGCT
Col1a1	CGTCTGGTTTGGAGAGAGCAT	GGTCAGCTGGATAGCGACATC
Bglap2	TGAGCTTAAGGGTGCTTGTGACGA	AGGGCAGCACAGGTCCTAAATAGT
Runx2	CGACAGTCCCAACTTCCTGT	CGGTAACCACAGTCCCATCT
HMGCoAR	CTTGTGGAATGCCTTGTGATT	AGCCGAAGCAGCACATGAT
CD36	GGAACTGTGGGCTCATTG	CATGAGAATGCCTCCAAACAC
Fatp3	AGGGTGACAGTGTTCCAGTACATT	TGGTCACACTCTGCCTTGCT
Cpt2	CCTGCTCGCTCAGGATAAACA	GTGTCTTCAGAAACCGCACTG
Acat1	CTACATGGGCAATGTCATCCA	TGCGCCCAGTGTTGCT

Pparg	GAGCTGGGTCTTTTCAGAATAATAAG	CAAGAATACCAAAGTGCGATCAA
Plin1	AGGCTGTCTCCTCTACCAAA	CCACAGTGTCTACCACGTTATC
Plin2	TTGAGATCCGTGTGTGAGATG	CCCTTGCAGGCATAGGTATT
Plin3	CTGGACAGACTGCAGGAAAG	CACTGTAGATGACACCAGTTCC
Plin4	CTGGTTACTAGGCTGCTGTAAG	GCTGTTGGTAGCCATGAGAT
Plin5	GCAGCTTCTCTTCCAATTTGTC	GTGTGTAGTGTGACTACCTGTG
Pgc1a	AACCACACCCACAGGATCAGA	TCTTCGCTTTATTGCTCCATG

Isolation of bone marrow stromal cells and culturing of osteoblasts

Primary murine bone marrow stromal cells (BMSCs) were isolated as previously described (43). Briefly, soft tissue was removed from freshly isolated femur and tibia at the distal and proximal ends. Total bone marrow was isolated by centrifugation at 12,000 rpm for 30 seconds and plated in complete α-MEM (α-MEM (Sigma, St. Louis, MO), 10% FBS (Avantor, Radnor, PA), and 1% penicillin/ streptomycin (Sigma, St. Louis, MO)). Then, these cells were incubated at 37°C with 5% CO_2. According to the plastic adherence theory, the adherent mesenchymal stromal cells stuck to the plastic flask while the non-adherent hematopoietic cells were washed away. This adherent cell population was then trypsinized after 48 hours, counted, and plated in appropriate tissue culture-treated plates at appropriate numbers. BMSCs were then cultured in osteogenic medium (complete α-MEM, 50 µg/ml ascorbic acid (Sigma, St. Louis, MO), and 5 mM β-glycerol phosphate (Sigma, St. Louis, MO) to induce osteoblast differentiation after the cells became 80% confluent (43).

Adipogenesis

BMSCs were differentiated into adipocytes for 7 d by using the adipogenic media previously described (43) with minor adjustments. Briefly, complete DMEM (α-MEM (Sigma, St. Louis, MO), 10% FBS (Avantor, Radnor, PA), 1% penicillin/ streptomycin (Sigma, St. Louis, MO)) was supplemented with 2 µM insulin (Sigma, St. Louis, MO), 0.5 mM 3-isobutyl-1-methylxanthine (IBMX) (Sigma, St. Louis, MO), 1 µM dexamethasone (Sigma, St. Louis, MO), and 20 µM rosiglitazone (Sigma, St. Louis, MO). Medium was changed every second day. After 96 hours, BMSCs were switched to complete high-glucose DMEM supplemented with 10% fetal bovine serum, 1% penicillin/streptomycin, 2 µM insulin, and 20 nM rosiglitazone. During differentiation, primary BMSCs were also cultured in the presence of

either DMSO (1%) or LAL inhibitor Lalistat 2 (0.1, 1, 10, and 50 μM; Tocris Bioscience, Boston, MA).

Alkaline phosphatase and Von Kossa staining

To determine how genetic deletion of LAL in osteoblast impacted their differentiation, BMSCs were isolated as described above. Isolated BMSc were pooled from either male of female Wt and bLal-/- mice, differentiated for 7 days, and stained for alkaline phosphatase (ALP) based on the manufacturer's protocol (Sigma, St. Louis, MO). Briefly, primary BMSCs (250×10^4 cells/ well) were cultured in osteoblast-differentiated medium for 7 days and stained for ALP. For this, cells were first washed with PBS 3 times, then fixed for 15 min with 10% neutral-buffered formalin (NBF), and then washed with H_2O twice. After addition of staining solution (500 μl) and incubation at RT for 10 min in the dark, the staining solution was aspirated and the cells were rinsed with H_2O for 5-6 times. For Von Kossa staining, cells were differentiated for 14 days, washed with H_2O, and then also fixed for 15 min with NBF. Thereafter, 2 ml/well of 5% silver nitrate solution was added to each well and the plate was exposed to strong UV light for 60 minutes, followed by incubation with 2 ml/well of 5% sodium thiosulfate solution for 2-3 minutes. Both methods included counterstaining using hematoxylin (500 μl) for 2 minutes. After that, cells were rinsed with tap water and air dried. The doses of Lalistat 2 were based both on previously published reports (33,44). Microscopic images were taken using a life technologies EVOS XL Core microscope (Thermo Scientific, Waltham, MA).

Oil Red O staining

To determine accumulation of neutral lipids in differentiated adipocytes, they were stained with oil red O (ORO). BM-Ads differentiated for 7 days were washed with PBS 3 times and fixed with 10% NBF for 20 min at RT. Thereafter, cells were washed with PBS. ORO (0.5 g) (Sigma-Aldrich, St. Louis, MO) was mixed with 100 μl isopropanol. ORO working solutions (30 mL of filtered stock and 20 mL ddH_2O, mixed for 10 min, filtered) was freshly prepared before use and added for 1 h. Microscopic images were taken using a life technologies EVOS XL Core microscope (Thermo Scientific, Waltham, MA).

Seahorse flux assays

ATP rate assay: To measure metabolic flux in real time by different seahorse-based assays, BM-Ads were plated in Seahorse XFe 96-well plates at 2.0×10^4 cells/well and cultured for

7 days with adipocyte differentiation medium. Cells were treated with Lalistat 2 using 1 and 50 μM concentration for 24 h (acute stress). DMSO (1%) implementation was performed as treatment of control cells.

Prior to the assay, the cells were washed with basal assay DMEM medium (Agilent, Santa Clara, CA) in the presence of 10 mM glucose, 2 mM glutamine, 1 mM sodium pyruvate, 200 nM insulin, and 60 μM oleic acid-BSA (all Sigma, St. Louis, MO) in the basal media. The sensor cartridge was hydrated overnight at RT instead of 37°C to minimize evaporation. Oxygen consumption rates (OCR) and extracellular acidification rates (ECAR) were then continuously monitored while tests were conducted using a final concentration of 2 μM oligomycin (Sigma, St. Louis, MO) and 1 μM rotenone/1 μM antimycin A (Sigma, St. Louis, MO). ECAR is mostly determined to quantify the percentage of glycolysis while considering the stoichiometry of the glycolytic pathway. In contrast, OCR that is suppressed by the addition of the ATP synthase inhibitor oligomycin can be used to quantify the rate of oxygen consumption linked to ATP generation during oxidative phosphorylation. The method concurrently evaluates the flux of H+ generation as seen in ECAR and O_2 consumption as shown in OCR. The rate of glycolysis and oxidative phosphorylation can be determined by gathering these data under basal circumstances and with successive administration of mitochondrial inhibitors (oligomycin and rotenone/antimycin A).

Statistical analysis

GraphPad Prism V9 was used to conduct statistical analyses. The Student's two-tailed unpaired t test was used to determine statistically significant differences between two groups, with significance set at $p < 0.05$. Data are expressed as mean + standard deviation (SD).

3. Results

3.1 Generation of osteoblast-specific Lipa-/- mice (bLal-/-)

Mice with ubiquitous *Lipa* gene deletion (Lal-/-, Lal ko) have already been investigated in detail. However, as was described above, this mouse model is insufficient to fully understand the function of LAL in bones due to potential systemic consequences of global LAL loss on the whole body, which may contribute to the skeletal phenotype. Thus, *Lipa* bone-specific, particularly osteoblast-specific knockout mice would be a suitable model to circumvent the issue of systemic LAL-D.

A LoxP-Cre approach was used (45) to allow inactivation of LAL specifically in osteoblasts. The selective production of Osteocalcin (OCN, also known as bone -carboxyglutamic acid protein, or Bglap) in differentiated osteoblasts allows for the targeting of the most mature/differentiated osteoblasts (46). OCN-Cre mice were obtained from Jackson Laboratory (Stock No 019509). Lipatm1a(EUCOMM)Hmgu/Biat mice were bred with FLP deleter mice (Taconic #7089) to produce a floxed Lipatm1c allele with restored *Lipa* expression ($Lipa^{fl/fl}$). Mice heterozygous for the floxed allele were crossed to produce homozygous $Lipa^{fl/fl}$ mice as controls. $Lipa^{fl/fl}$ mice were then bred with transgenic OCN-Cre mice expressing the Cre recombinase under the control of the *Bglap* (OCN) promoter to generate bone-specific $Lipa^{fl/fl}$ OCN-$Cre^{+/-}$ mice. Mice containing the osteoblast-specific deletion were then bred to produce $Lipa^{fl/fl}$ OCN-$Cre^{+/+}$ (bLal-/-, Ko) or $Lipa^{fl/fl}$ OCN-$Cre^{-/-}$ (Wt) as respective control littermates. Additional genotyping in the laboratory confirmed genotypes in bLal-/- mice (Figure 1).

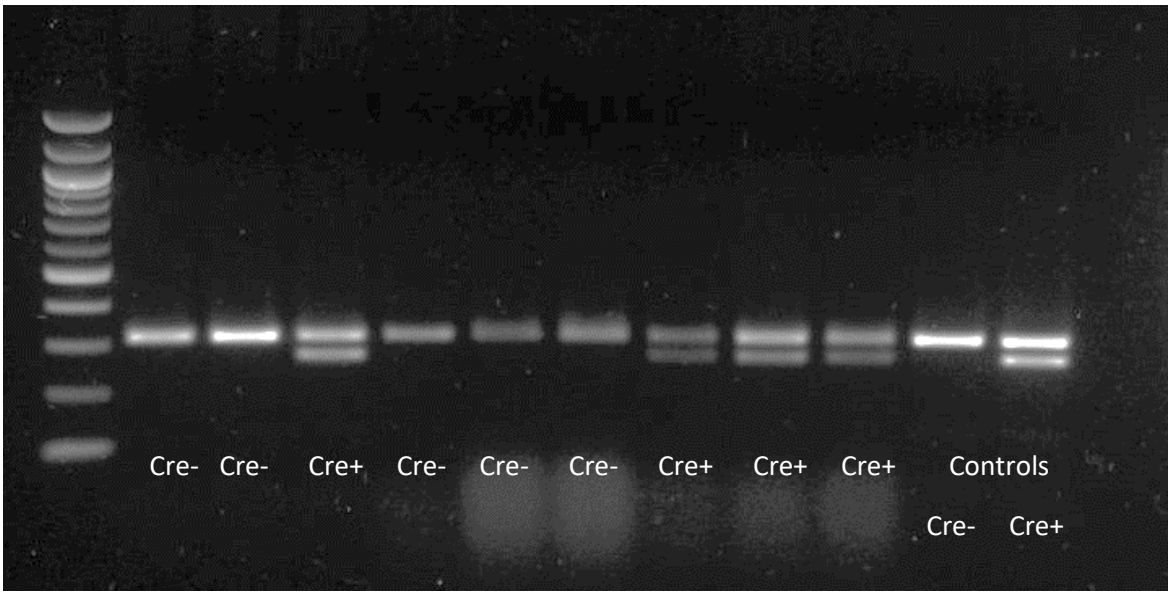

Figure 1. Lipa$^{fl/fl}$ OCN-Cre$^{+/+}$ (bLal-/-) and Lipa$^{fl/fl}$ OCN-Cre$^{-/-}$ (Wt) mice genotyping. Representative image of DNA gel with fluorescently labeled PCR products. For Lipa $^{fl/fl}$ OCN-Cre$^{-/-}$ (Cre-) mice expected product is 324bp, while for Lipa$^{fl/fl}$ OCN-Cre$^{+/+}$ (Cre+) is 280 and 324bp.

3.2 Significantly reduced *Lipa* mRNA in male but not in female bLal-/- mice

Levels of *Lipa* mRNA expression in bones in 3 of 5 bLal-/- mice were reduced by ~ 50% compared to control mice (Figure 2A). However, we were only able to detect a successful recombination in 1 female mouse out of 5 tested. Additionally, we performed an LAL fluorescent activity assay, which revealed functionally active LAL in bLal-/- female mice. These data suggested that despite appropriate genotyping results, recombination was not fully efficient, at least in the studied female Lipa$^{fl/fl}$ OCN-Cre$^{+/+}$ mice.

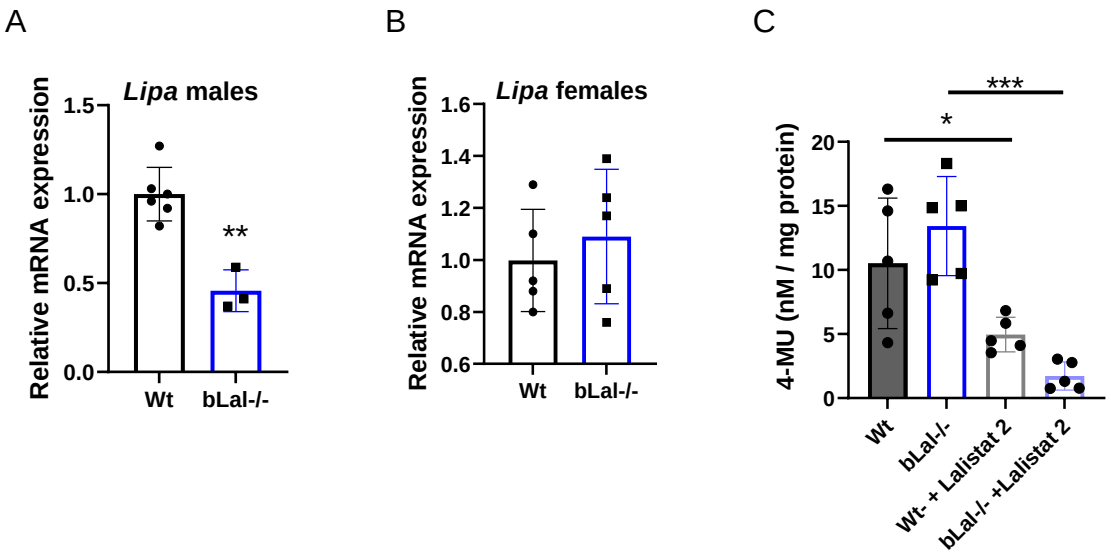

Figure 2. LAL is efficiently knocked out in osteoblast of male but not in female bLal-/- mice.

Lipa mRNA expression relative to *cyclophilin A* as reference gene in chow fed 16-week-old (A) male (Wt, n=6; Ko, n=3) and (B) female (Wt, n=5; Ko, n=5) mice in flushed tibia. (C) LAL activity in flushed tibias of bLal-/- and respective Wt (n=5) female mice was determined using the fluorogenic substrate 4-MUP at pH 4 in the absence or presence of Lalistat 2. Data represent means ± SD; $p < 0.05$ (*), $p \leq 0.01$ (**), $p \leq 0.001$ (***). Student's unpaired t-test.

3.3 Knockout of LAL in osteoblast does not affect body weight and body composition of mice

We failed to identify any difference in body weight of either male (Figure 3A) or female mice (Figure 3B) at all studied ages. Bone mineral content (BMC) in both male (842mg ± 94.7) and female (604.37mg ± 34.13) mice were comparable (Figure 3C, D), as well as density (BMD) (males: 84mg/cm2 ± 8.884; females:74.19mg/ cm^2 ± 2.15) (Figure 3E, F) to control littermates (male: 725mg ± 99.57; females: 616.67mg ± 30.77) and (males: 81mg/ cm^2 ± 7.4; females: 75.54 mg/cm^2 ± 1.99) respectively at 16 weeks of analysis. No changes in fat (males: 4.2g ± 1.4 vs 4.88g ± 1.2; females: 2.85m ± 1.03 vs 2.97g ± 0.84) or lean (males: 22.27g ± 2.5 vs 23.6g ± 3.01; females: 18.16g ± 1.28 vs 17.8g ± 0.79) mass were found in both sexes (Figure 3G-J) at the end of experiment. The length of tibia from both males and females was also stable between genotypes (males: 17.58mm ± 0.48 vs 17.44± 0.26; females: 17.41mm ± 0.41 vs 17.75mm ± 0.52) (Figure 3K, L).

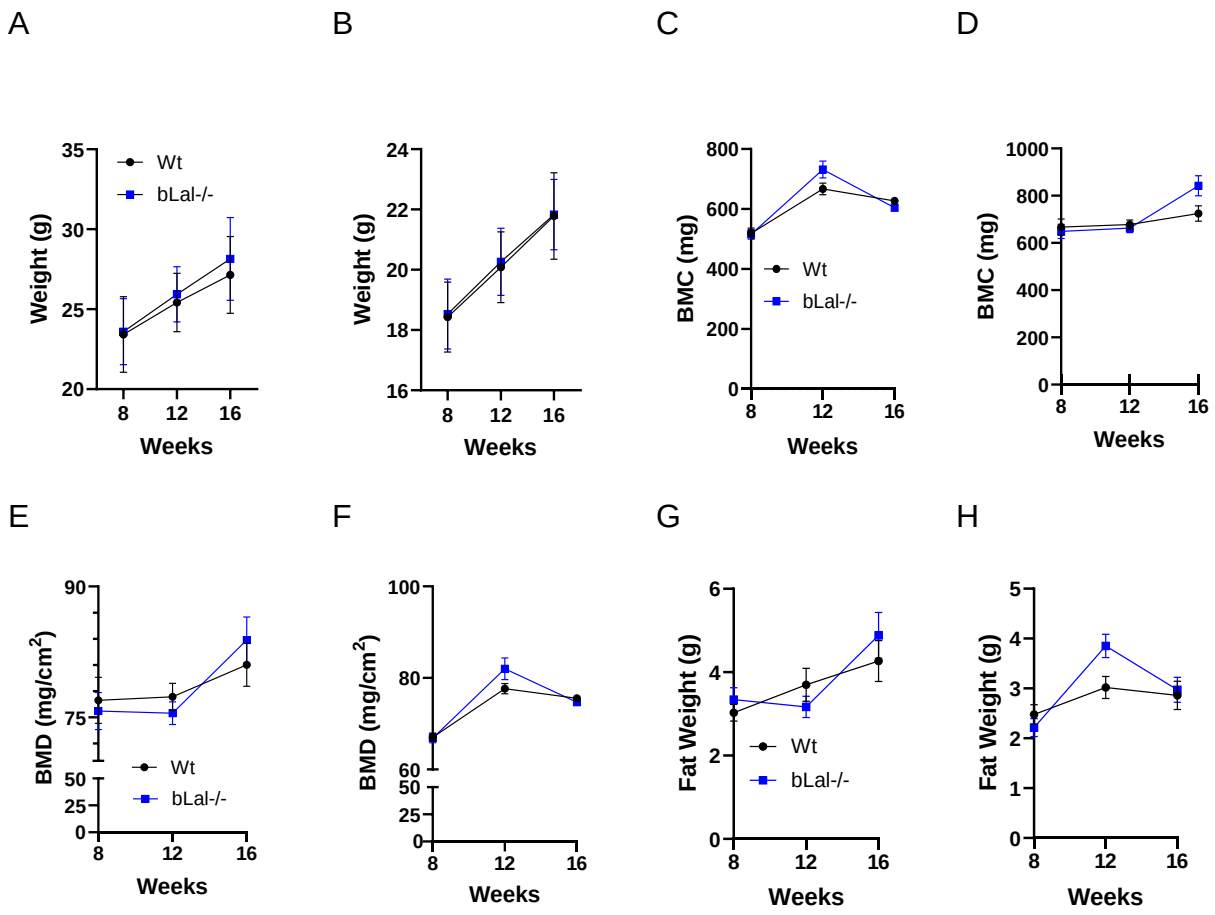

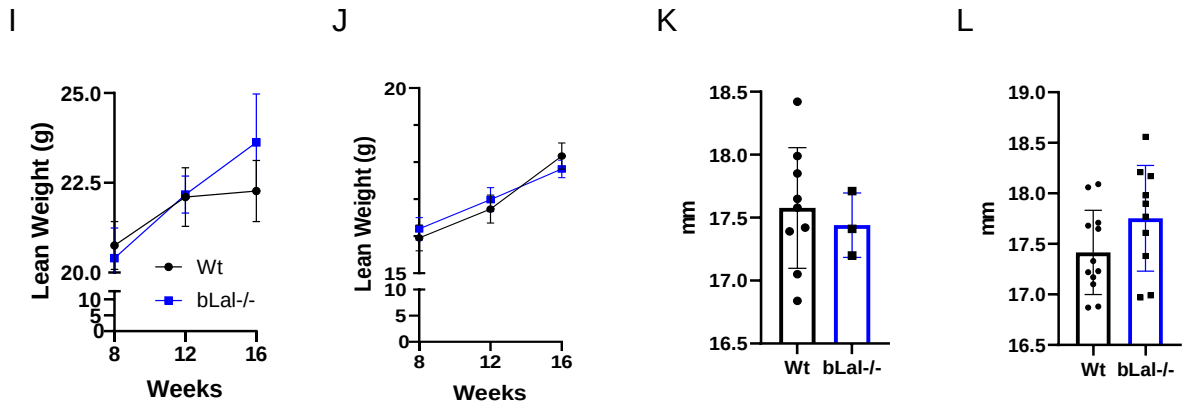

Figure 3. Comparable body weight as well as body and bone composition in Wt and bLal-/- male and female mice.

Body weights of chow-fed 16-week-old (A) male (Wt, n=6; Ko, n=3-5) and (B) female (Wt, n=13; Ko, n=11) mice. (C-J) Analysis of Dual energy X-ray absorptiometry (DXA) scanning of whole body; (C, D) Bone mineral content (BMC; mg). (E, F) Bone mineral density (BMD; mg/cm^2). (G, H) Fat weight of the animal (g). (I, J) Lean weight of the animal (g). (C, E, G, I) chow-fed 16-week-old (A) males (Wt, n=6; Ko, n=3-5). (D, F, H, J) females (Wt, n=13; Ko, n=11). The length of tibia from (K) male (Wt, n=6; Ko, n=3) and (L) female (Wt, n=13; Ko, n=11) mice. Data represent mean ± SD. Student's unpaired t-test.

3.4 Comparable cortical bone phenotype in chow diet-fed control and bLal-/- mice

The cortical bone parameters measured by the µCT analyses revealed similar parameters in male bLal-/- and Wt mice. In detail, cortical area (Ct.Ar.), total cross-sectional area (Tt. Ar.), cortical tissue mineral density (Ct. TMD) as well as cortical thickness (Ct.Th.), and cortical porosity (Ct.Po.) were identical to respectful measurements in Wt male littermates (Figure 4A, C, E, G, I).

Female bLal-/- mice likewise displayed similar cortical parameters when compared to Wt including cortical area (Figure 4B), thickness (Figure 4G), mineral density (Figure 4F), porosity (Figure 4J) as well as total area (Figure 4D). Interestingly, female but not male bLal-/- mice demonstrated decreased moment of inertia (MMOI) (Figure 4L) suggesting reduced biomechanical strength (Figure 4K). Lack of change between the genotypes was also noted in the bone marrow volume (Figure 2M, N).

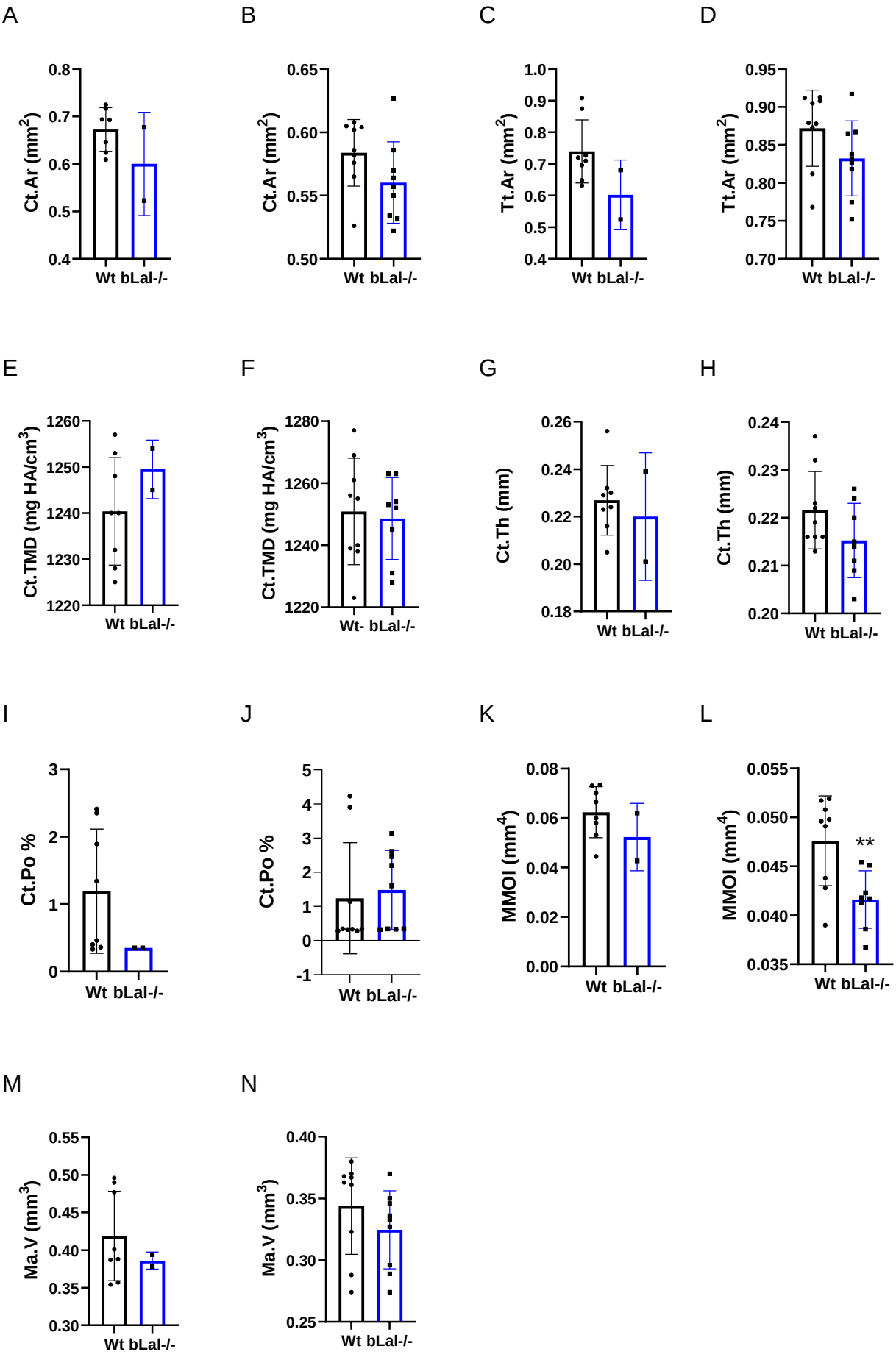
A
Ct.Ar (mm2)
0.8
0.7
0.6
0.5
0.4
Wt bLal-/-
B
Ct.Ar (mm2)
0.65
0.60
0.55
0.50
Wt bLal-/-
C
Tt.Ar (mm2)
1.0
0.9
0.8
0.7
0.6
0.5
0.4
Wt bLal-/-
D
Tt.Ar (mm2)
0.95
0.90
0.85
0.80
0.75
0.70
Wt bLal-/-
E
Ct.TMD (mg HA/cm3)
1260
1250
1240
1230
1220
Wt bLal-/-
F
Ct.TMD (mg HA/cm3)
1280
1260
1240
1220
Wt- bLal-/-
G
Ct.Th (mm)
0.26
0.24
0.22
0.20
0.18
Wt bLal-/-
H
Ct.Th (mm)
0.24
0.23
0.22
0.21
0.20
Wt bLal-/-
I
Ct.Po %
3
2
1
0
Wt bLal-/-
J
Ct.Po %
5
4
3
2
1
0
-1
Wt bLal-/-
K
MMOI (mm4)
0.08
0.06
0.04
0.02
0.00
Wt bLal-/-
L
MMOI (mm4)
0.055
0.050
0.045
0.040
0.035
**
Wt bLal-/-
M
Ma.V (mm3)
0.55
0.50
0.45
0.40
0.35
0.30
Wt bLal-/-
N
Ma.V (mm3)
0.40
0.35
0.30
0.25
Wt bLal-/-

Figure 4. Reduced minimum moment of inertia in female bLal-/- mice despite no change in other cortical parameter neither in male no in female mice.

Micro-computed tomography (µCT) analysis of the cortical bone assessed at the tibia diaphysis. (A, B) Cortical bone area (Ct.Ar.); (C, D) total area; (E, F) cortical tissue mineral density; (G, H) cortical thickness (Ct.Th.); (I, J) cortical Porosity (Ct.Po.); (K, L) minimum moment of inertia (MMOI); and (M, N) Bone marrow volume (Ma.V.). (A, C, E, G, I, K, M) chow-fed 16-week-old males (Wt, n=8; Ko, n=2). (B, D, F, H, J, L, N) females (Wt, n=10; Ko, n=10). Data represent mean ± SD; $p \leq 0.01$ (**). Student's unpaired t-test.

3.5 Reduced trabecular thickness and mineral density in female but not in male bLal-/- mice

As µCT analyses of the tibia diaphysis failed to identify any difference in the investigated parameters between the bLal$^{-/-}$ and Wt mice, we further studied tibia metaphysis in male mice as quantitated by Bb.BV/TV (Figure 5A), connectivity density (Tb. Conn.Dens.) (Figure 5C), trabecular number (Tb. N.) (Figure 5E), separation (Tb.Sp.) (Figure 5G), thickness (Tb.Th.) (Figure 5I), and trabecular tissue mineral density (Tb. TMD) which were unchanged in between genotypes. Surprisingly, bLal-/- females exhibited reduced Tb.Th. (Figure 5J) and Tb. TMD (Figure 5L) compared to control littermates. However, we cannot speculate affected trabecular phenotype in those mice since other trabecular parameters such as Bb.BV/TV, Tb. N., and Tb.Sp. were unchanged (Figure 5 B, D, F, H). Structure Model Index (SMI) remained comparable between mice of different genotypes and/or sex (Figure 5M, N).

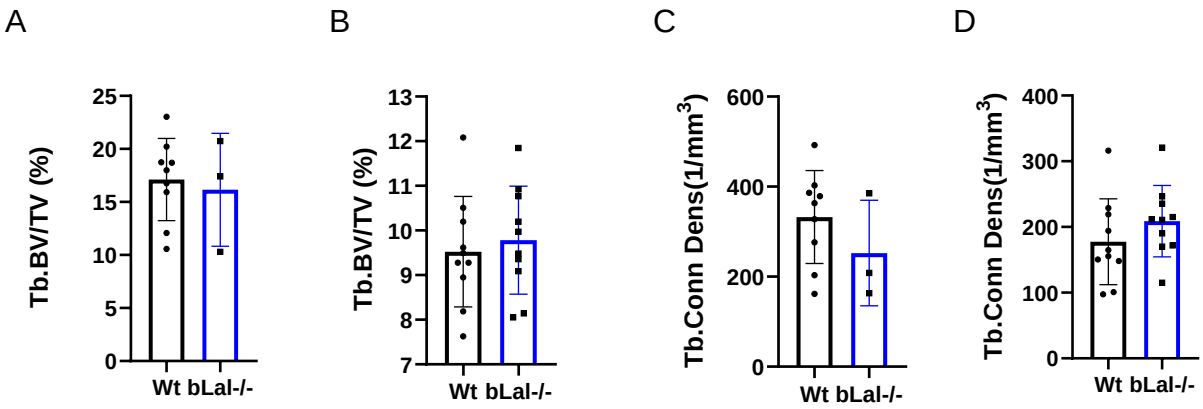

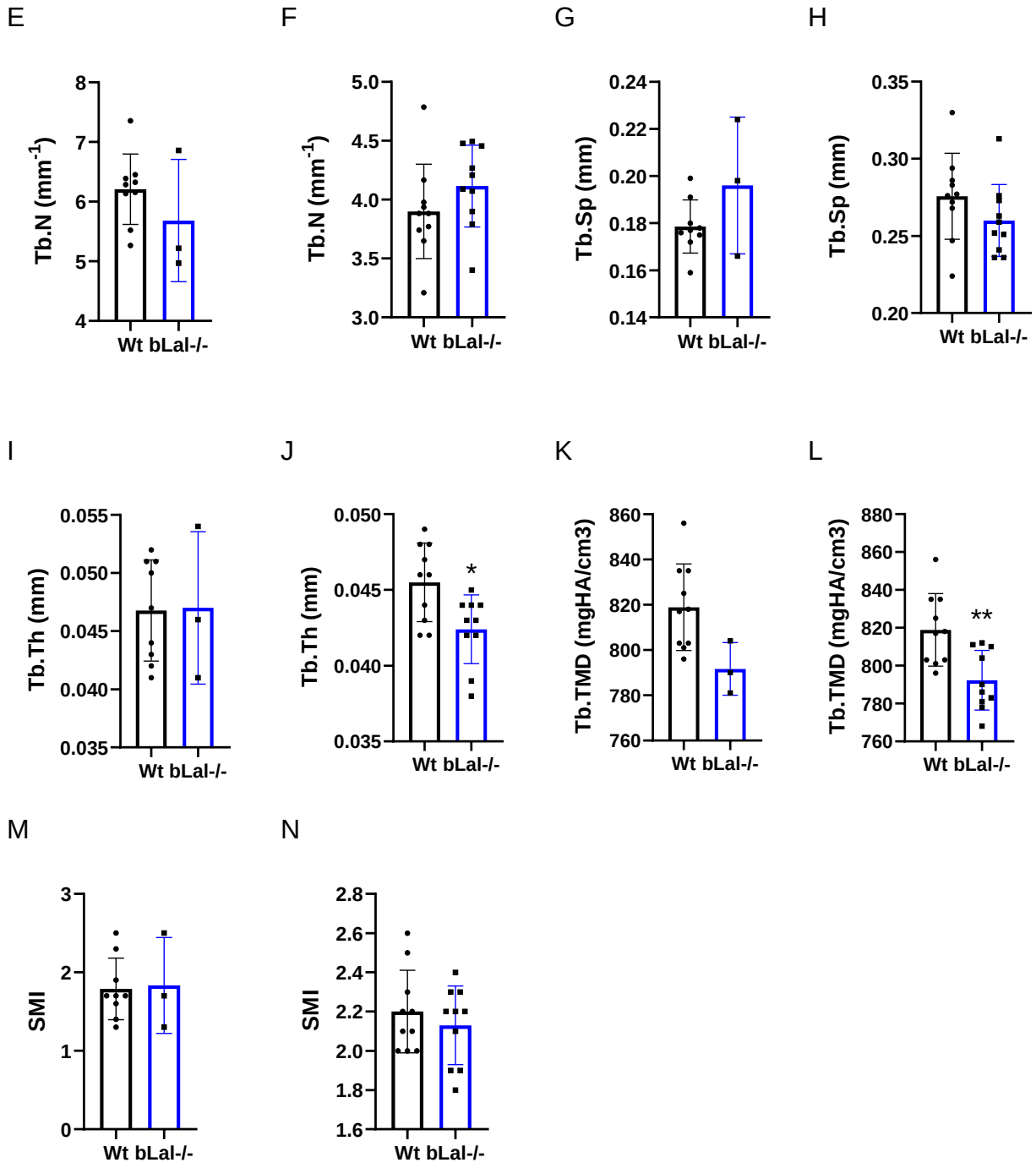

Figure 5. Decreased trabecular parameters in female bLal-/- mice despite no changes in male's metaphysis.

Micro computed tomography (µCT) analysis of trabecular bone quantified in (A, B) Percentage bone (trabecular) volume over total volume (Tb. BV/TV); (C, D) Connection density (Tb. Conn. Dens.); (E, F) Trabecular number (Tb. N); (G, H) Trabecular separation (Tb.Sp.); %).; (I, J) Trabecular thickness (Tb. Th.); (K, L) tissue mineral density (Ct.TMD), and (M, N) structure model index (SMI). (A, C, E, G, I, K, M) represent data from chow-fed

16-week-old males (Wt, n=9; Ko, n=3) and (B, D, F, H, J, L, N) females (Wt, n=10; Ko, n=10). Data represent mean ± SD; $p < 0.05$ (*), $p \leq 0.01$ (**). Student's unpaired t-test.

3.6 Knockout of LAL in the osteoblast failed to affect the expression of bone marker genes

Followed the observations of comparable cortical and trabecular bone parameters in male and minor differences in female mice, we performed a qPCR to estimate main bone development- and "well-being"-related genes. As expected, we failed detect alterations in those gene markers either in male (Figure 6A) or in female (Figure 6B) bLal-/- mice compared to their Wt controls.

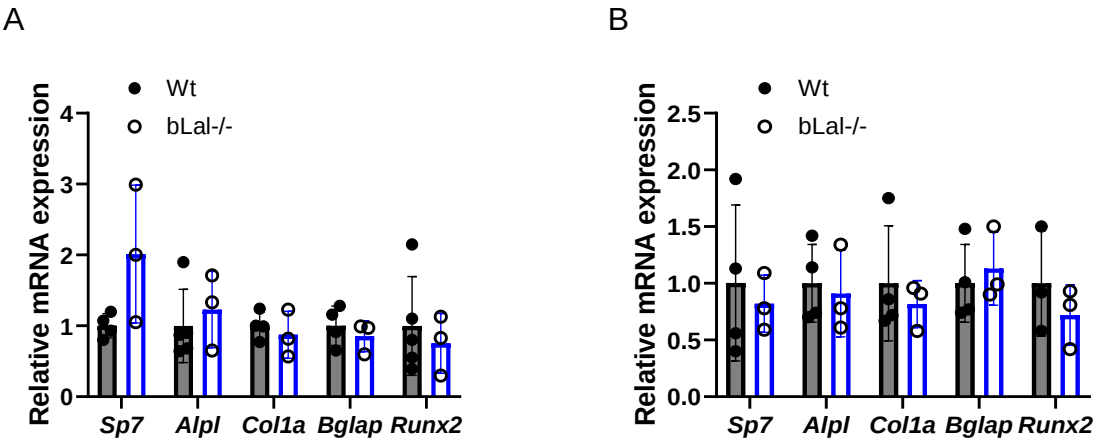

Figure 6. Unaltered expression of mane bone markers in bLal-/- mice. qPCR analysis of osteogenic differentiation-related markers (in flushed femurs) in chow-fed 16-week-old (A) males (Wt, n=4-5; Ko, n=3) and (B) females (Wt, n=3-4; Ko, n=3). Data represent mean ± SD. Student's unpaired t-test.

3.7 Similar bone lipid content in bLal-/- and Wt mice

To investigate whether loss of LAL in osteoblasts affects lipid composition of bones, we extracted lipids from flushed tibias i.e, from bone without bone marrow. We performed a thin-layer chromatography of the extracted lipids and found comparable amount of TG and CE in bLal-/- mice and their correspondent littermates in both male (Figure 7A, C, E) and female animals (Figure 7B, F, H). Similar finding occurred for free fatty acids isolated from long bones of 16-week-old mice of both sexes (Figure 7D, G). Relative expression of various lipid metabolism relented genes was also comparable between the genotypes in both male and female mice (Figure 7I, J).

A

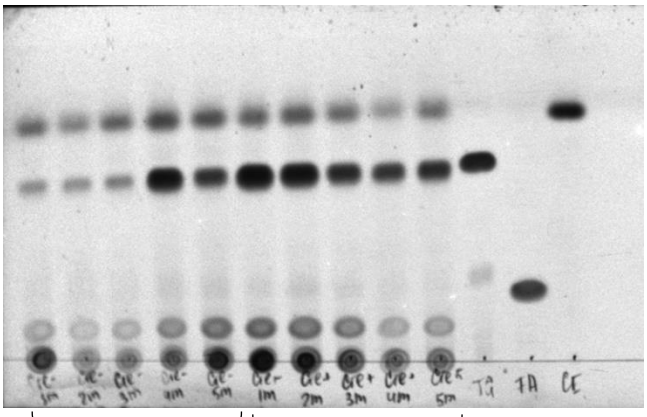
TG FA CE
Cre-(Wt)
Cre+(bLal-/-)
standards

B

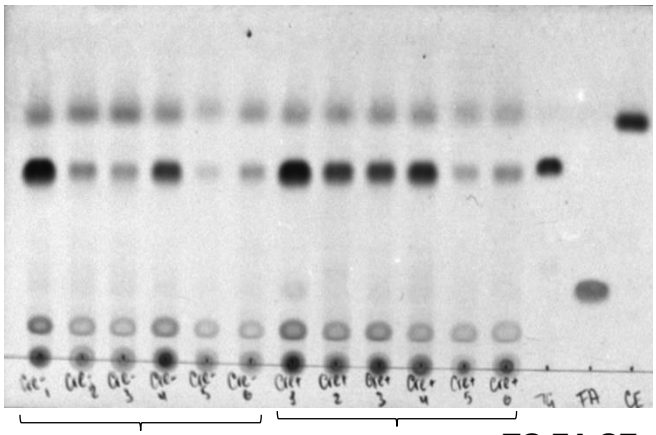
TG FA CE
Cre-(Wt)
Cre+(bLal-/-)
standards

C

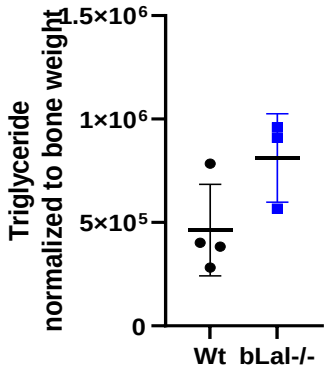
Triglyceride
normalized to bone weight
1.5×10⁶
1×10⁶
5×10⁵
0
Wt
bLal-/-

D

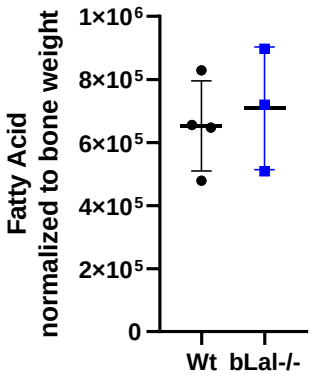
Fatty Acid
normalized to bone weight
1×10⁶
8×10⁵
6×10⁵
4×10⁵
2×10⁵
0
Wt
bLal-/-

E

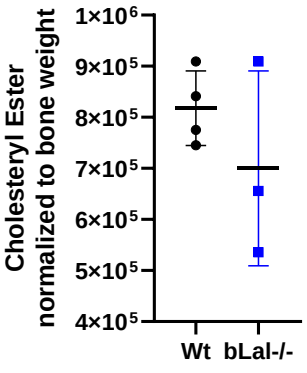
Cholesteryl Ester
normalized to bone weight
1×10⁶
9×10⁵
8×10⁵
7×10⁵
6×10⁵
5×10⁵
4×10⁵
Wt
bLal-/-

F

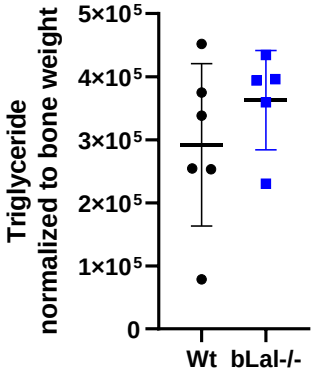
Triglyceride
normalized to bone weight
5×10⁵
4×10⁵
3×10⁵
2×10⁵
1×10⁵
0
Wt
bLal-/-

G

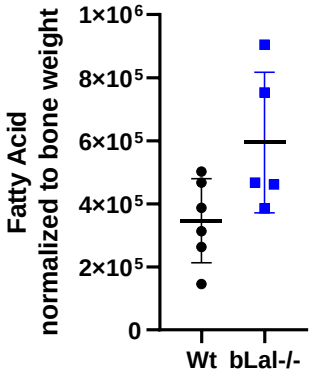
Fatty Acid
normalized to bone weight
1×10⁶
8×10⁵
6×10⁵
4×10⁵
2×10⁵
0
Wt
bLal-/-

H

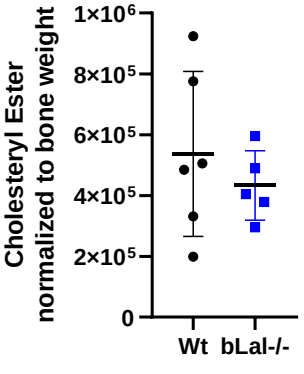
Cholesteryl Ester
normalized to bone weight
1×10⁶
8×10⁵
6×10⁵
4×10⁵
2×10⁵
0
Wt
bLal-/-

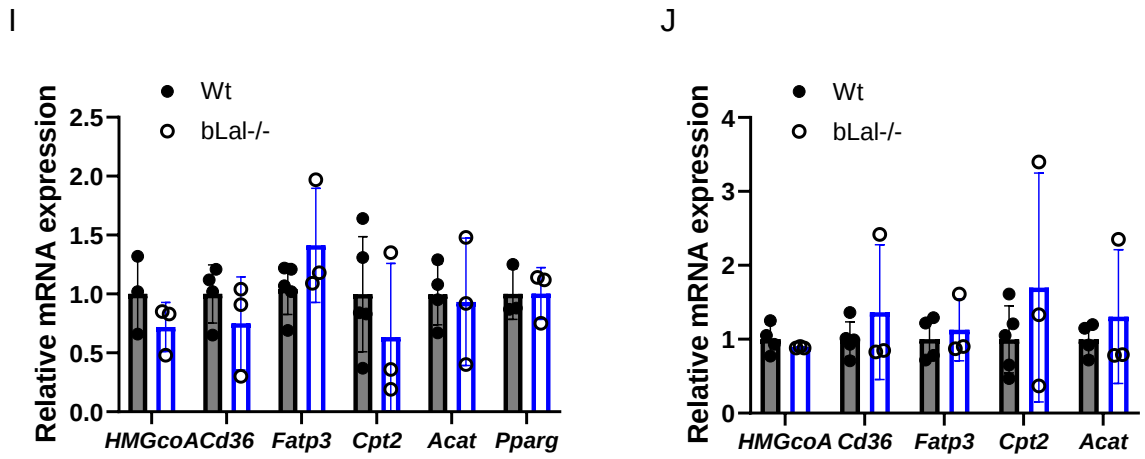

Figure 7. Loss of LAL in osteoblasts does not affect lipid metabolism and storage in bones. Thin layer chromatogram of lipids harvested from flushed tibia (tibia without any bone marrow) from 16-week-old (A) male and (B) female mice. Densitometric quantification of (C, F) TG, (D, G) fatty acid, and (E, H) CE normalized to bone weight. (C, D, E) represent data from fed 16-week-old males (Wt, n=4; Ko, n=3) and (F, G, H) females (Wt, n=5; Ko, n=5). mRNA expression of various lipid metabolism-related genes in of chow diet-fed male (I) (Wt, n=3-4; Ko, n=3) and female (J) (Wt, n=4-5; Ko, n=3) Wt and bLal-/- mice. Data represent mean ± SD. Student's unpaired t-test.

3.8 Unaltered osteoblastogenesis in BMSc isolated from bLal-/- and Wt mice

Even though we could not observe any drastic changes in the expression of the gene responsible for bone development (Figure 6A, B) we performed a series of experiments with BMSCs isolated from tibias and femurs of bLal-/- and their corresponding littermates. Cells from both male and female mice differentiated with osteogenic medium for 7 days failed to exhibit impaired differentiation potential, as indicated by comparable ALP staining (Figure 8A). Similar hematoxylin staining was noted between Ko and Wt cells (Figure 4A), which confirms no changes at an early stage of osteoblast differentiation. Further, the calcification of the matrix in BMSCs was evaluated using the von Kossa stain. Within the cell monolayer, dark-brown patches that represented calcification were quantitated to confirm osteogenic differentiation. Stromal cells isolated from Ko mice exhibit lover percentage of stained area, which, however, correlated with lower intensity of hematoxylin staining in those cells (Figure 8B). Additionally, comparable BMSCs differentiation capacity was confirmed by unaltered expression of osteogenic differentiation-related markers (Figure 8C) from BMSCs isolated from flushed bones of female mice.

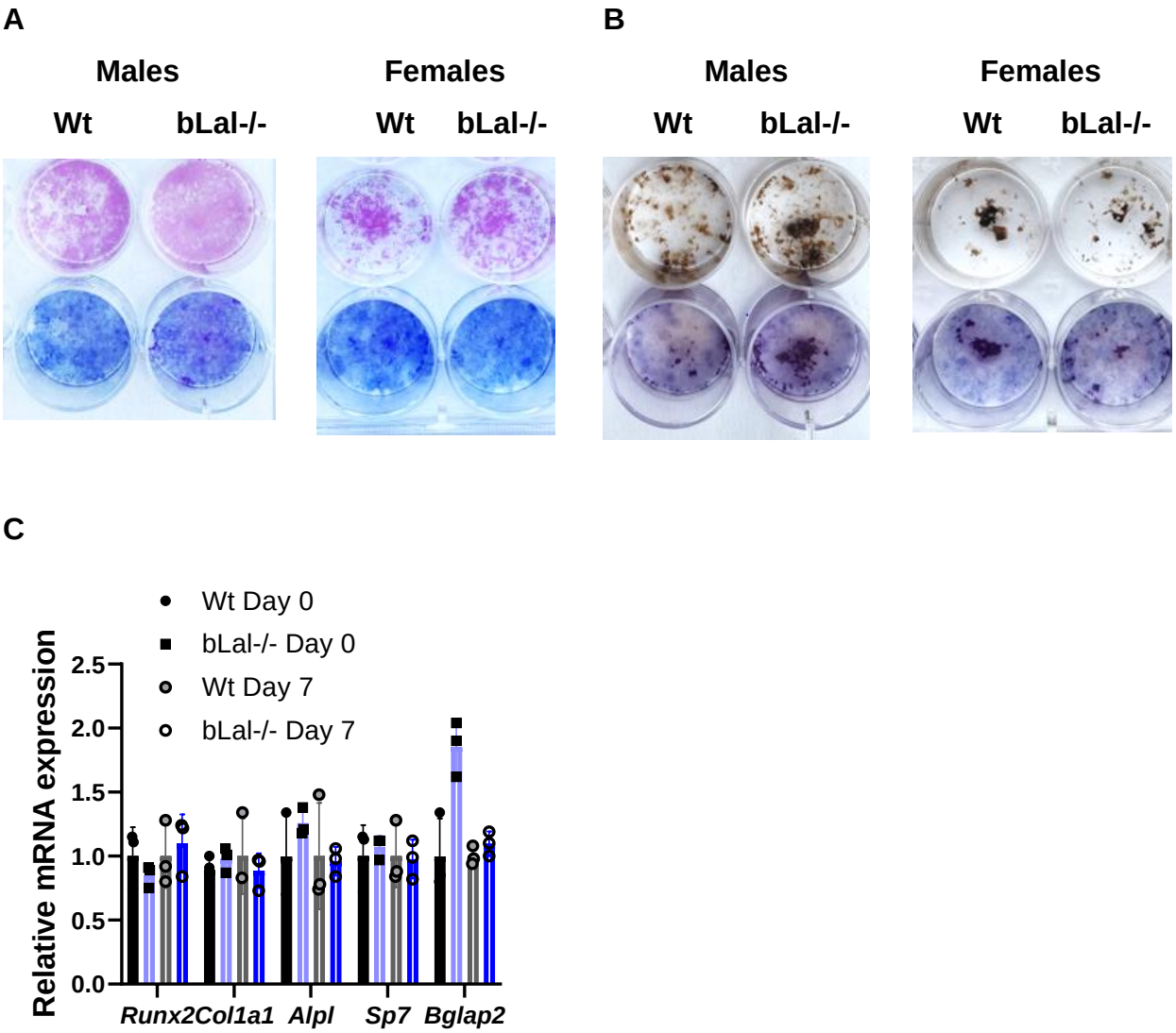

Figure 8. Comparable osteoblastogenesis in BMSCs isolated from bLal-/- and Wt mice. (A) Representative images of Wt and bLal-/- primary bone marrow stromal cells (BMSCs) after 7 days of osteoblast differentiation stained for ALP and hematoxylin, and (B) 14 days of osteoblast differentiation stained for von Kossa and hematoxylin. (C) mRNA expression of various osteogenic marker genes of chow diet-fed female (Wt, n=3-4; Ko, n=3) Wt and bLal-/- mice. Data represent mean ± SD. Student's unpaired t-test.

3.9 Lalistat 2 treatment of BM-derived adipocytes increases adipogenesis

Another approach to investigate the role of LAL in skeletal niche includes experiments with BM-Ads treated with LAL inhibitor Lalistat 2. However, a recent study (44) hints that in addition to LAL, the compound inhibits key cytosolic neutral lipid hydrolases involved in lipid droplet breakdown in primary cells via its off-target actions. As a result, interpreting inhibitor effects on lipid metabolism should be done with caution, and inhibitor doses used in cell culture studies should be tested individually for each cell line and generally not exceed 1 µM

concentration (44). Due to this, we performed a treatment of BM-Ads with a serial dilution of Lalistat 2 including 0.1, 1, 10 (results are not shown), and 50 µM.

ORO staining revealed increased natural lipid accumulation in BM-Ads after 7 days of differentiation with increasing concentrations of Lalistat 2 (Figure 9A). By estimating the expression of the main lipid droplets markers, we confirmed that Perilipin 2 was the most abundant perilipin in BM-Ads (Ct~18 versus *Plin1,* Ct~21; *Plin,3* Ct~24; *Plin4,* Ct~23, and *Plin 5*, Ct~28-29) (Figure 9B). A trend to increased expression of *Plin2* and *Pparg (γ)* may indicate enhanced adipogenesis in these cells, even upon treatment with low Lalistat 2 dose (Figure 9B).

A

DMSO

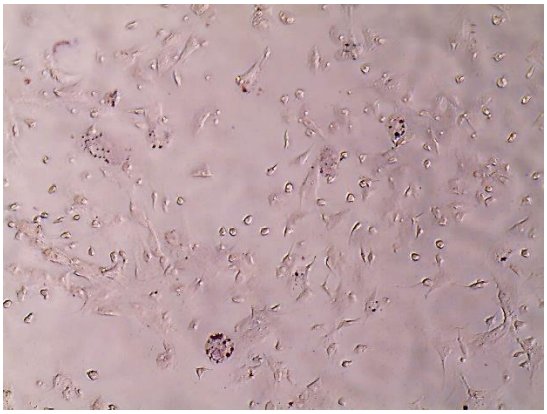

Lalistat 2 0.1 µM

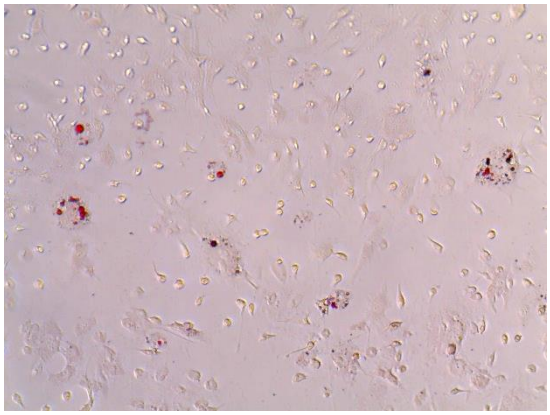

Lalistat 2 1 µM

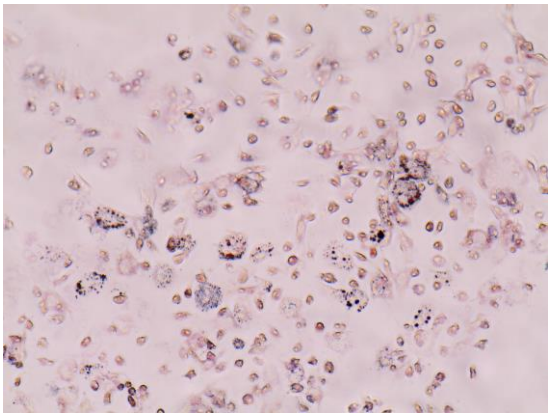

Lalistat 2 50 µM

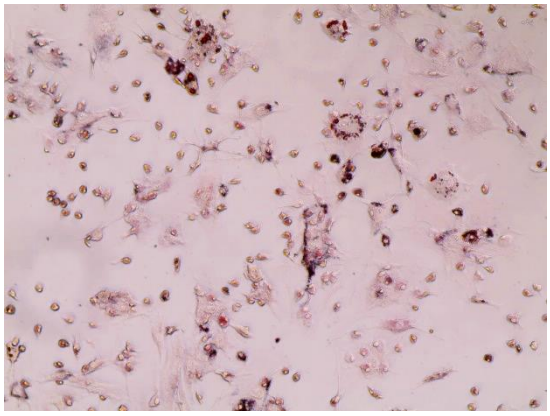

B

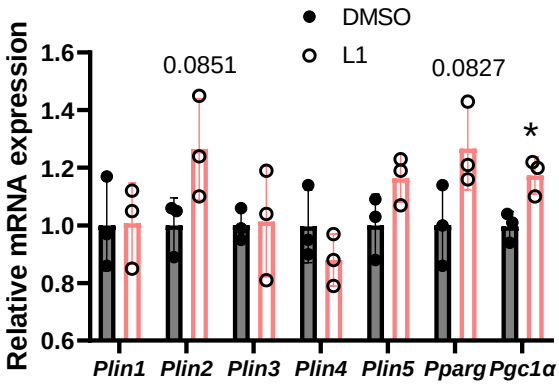

Figure 9. Lalistat 2 treatment of BM-derived adipocytes increased lipid accumulation and expression of adipogenic markers. (A) Representative images (bright field, 20x) of control (DMSO treated) and Lalistat-2 treated bone marrow-derived adipocytes (BM-Ads) after 7 days of differentiation stained with Oil red O (ORO). (B) mRNA expression of various lipid droplet marker genes in BM-Ads treated with either DMSO or 1 µM Lalistat 2 (L1) (n=3). Data represent mean ± SD; $p < 0.05$ (*). Student's unpaired t-test.

3.10 Lalistat 2 treatment alters ATP production in BM-derived adipocytes, but not osteoblasts

To determine how LAL inhibition influences the bioenergetic status and metabolic profile of cells during osteoblast- and adipogenesis, BMSCs were differentiated to osteoblasts and adipocytes for 6 days followed by 24h Lalistat 2 (1 or 50 µM) or DMSO treatment. Impairing LAL in osteoblasts reduces ATP production rates only upon incubation with 50 µM, but not 1 µM of Lalistat 2 (Figure 10). Unexpectedly, treatment of BM-Ads with 1 µM Lalistat 2 caused a shift towards a more glycolytic phenotype. With increasing concentrations of Lalistat 2, adipocytes drastically reduced mitochondrial ATP production, leading to decreased total ATP output (Figure 10).

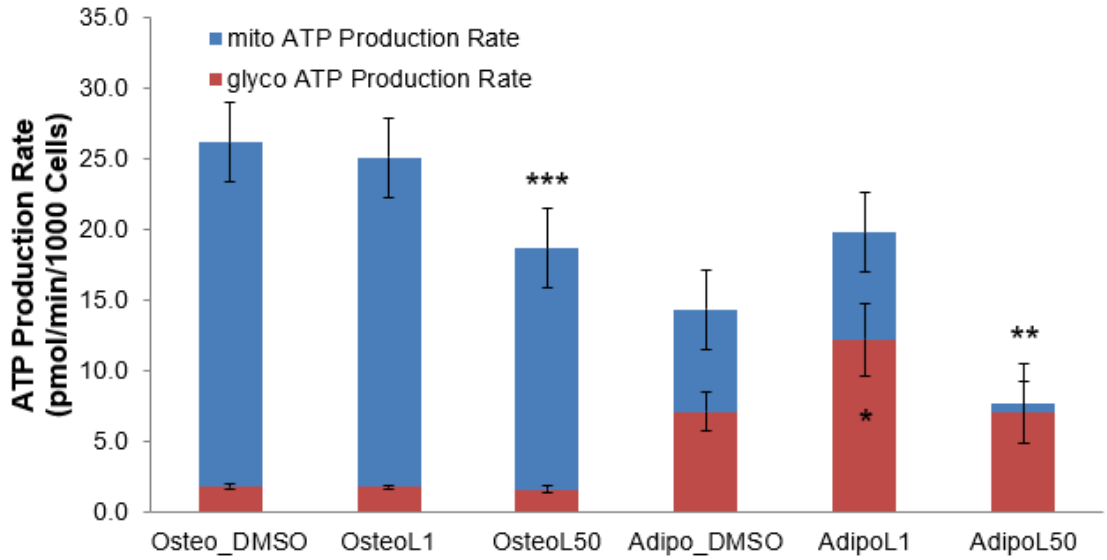

Figure 10. Increased glycolytic ATP production in adipocytes but not osteoblasts treated with 1 µM Lalistat 2. ATP production rates assessed by the Seahorse Flux analysis in bone marrow derived osteoblasts (Osteo) or adipocytes (Adipo) treated with either DMSO, 1 µM Lalistat 2 (L1), or 50 µM Lalistat 2 (L50). Data represent mean ± SD; $p < 0.05$ (*), $p \leq 0.01$ (**), $p \leq 0.001$ (***) compared to DMSO control. One-way ANOVA.

4. Discussion and limitations

LAL-D is a potentially fatal condition that has attracted a lot of attention in the recent decade. The syndrome is distinguished by a significant CE and TG buildup in several organs as well as premature death (23,25,47–49). We previously discovered that Lal-/- mice of both sexes have detrimental long bone phenotype, resulting in inferior biomechanical qualities (33). Furthermore, we concluded that LAL depletion has a significant clinical impact on fracture risk (33) and hypothesized that LAL regulation of lipid metabolism may be essential for proper osteoblast function. To reveal the mechanism of the impaired bone metabolism in LAL-D we employed Lipa$^{fl/fl}$ OCN-Cre mouse model (LAL osteoblast-specific knockout mice).

Osteocalcin (OCN)-Cre transgenic lines were generated to drive Cre expression in mature osteoblasts. It is known that Cre lines can exhibit off-target behaviors in both somatic tissues and germline cells (50). Cre activity in the latter is problematic since it will result in the loss of the Cre transgene/knock-in's intended targeting function and transmission of the recombined floxed allele to the carrier's offspring (51,52). Importantly, Cre-mediated reporter activity could not correctly reflect the targeted floxed gene's recombination efficiency since various gene loci may respond differently to Cre-mediated recombination (50). Osteocalcin is known to be a marker of mature osteoblast and osteocytes. In humans OCN promoter itself is initially activated during intrauterine life which makes this promoter not suitable enough for gene inactivation during early bone development (53–55). However, a few studies reported Cre recombinase activity in skull vault osteoblasts (56,57), trabecular osteoblasts, and osteocytes of 6-week-old mice using OCN-cre transgenic mice. Unfortunately, in our Lipa$^{fl/fl}$ OCN-Cre+ female mice, LAL expression as well as activity was detected in flushed femurs of 4 out of 5 studied mice. It is known that extracellular LAL can be taken up by other cells through M6P receptor-mediated endocytosis, and remain catalytically active (58–60). Although this does not explain unchanged mRNA expression since it should be reduced independent of the protein uptake. Thus, consequently obtained changes in female mice, for instance in trabecular thickness and trabecular mineral density, should be regarded with caution as a possible side effect of Cre recombinase.

Even though, we were able to confirm reduced expression of *Lipa* in 3 out of 5 studied Lipa$^{fl/fl}$ OCN-Cre+ male mice, we could not observe any significant changes either in bone parameters or in lipid content and metabolism of examined animals. This may not be surprising, as some tissue-specific LAL ko models, (e.g. small intestine-(enterocytes)

specific), despite a relatively high LAL expression failed to maintain ectopic lipid accumulation typical for global LAL-ko mice, as it was likely not caused by the loss of the enzyme in the respective tissue, but rather the lipid enrichment in infiltrating macrophages (32). However, it is still elusive whether the absence of changes in bLal-/- mice is due to low sample size in our experimental setup or the lack of effect from the loss of LAL specifically in osteoblasts, which requires further studies.

The expression of LAL in BM-Ad cells is quite high, but the exact role of LAL in BM-AT remains elusive (34). Interestingly, BM-Ads have a unique lipid metabolism since they lack classical lipolytic degradation of cytosolic lipid droplets by adipose triglyceride lipase and exhibit a cholesterol-orientated metabolism. Thus, BM-Ads could be an important source of cholesterol and related metabolites. Therefore, we studied whether LAL is involved in cholesterol homeostasis in BM-Ads. BM-Ads treated with Lalistat 2 exhibit increased lipid accumulation with increasing LAL inhibitor concentration.

Interestingly, PLIN1 has previously been identified in marrow adipocytes both using immunohistochemistry and western blot analysis (61). Our study, however, reveals that *Plin2*, which is also upregulated during adipocyte differentiation (62), is the most abundant type of perilipins in bone marrow derived adiposities. Increased expression of adipogenic markers Pparg (γ), which is also known to be essential in adipocyte differentiation (63,64), coupled with lipid storage, hint that Lalistat 2 treatment of BM-Ads improves adipogenesis. However, to validate current findings, we must confirm that the concentration of the inhibitor was specific for studied cell type, which requires further experiments.

Finally, we tested how bone marrow derived osteoblasts and adipocytes use their substrates to generate ATP in the conditions of LAL inhibition. Unexpectedly, BM-Ad preferred glycolysis to oxidative phosphorylation, whereas white adipocytes principally use terminal oxidation to generate ATP (64). Differences in Lalistat 2 treated cells were even more pronounced, suggesting that upon treatment, BM-Ads utilize more glucose for energy production. Opposing, BM-derived osteoblasts exhibited more OXPHOS-based metabolism unaffected with a small dose of Lalistat 2. However, we were able to find overall impaired ATP production in both cell types only when a high concentration of Lalistat 2 was used, which was described as unspecific (44) and thus these findings should be taken with caution.

5. Future directions

To target osteoblasts throughout their differentiation program, in future studies Prrx1-Cre.Lipa$^{fl/fl}$ and DMP1-Cre.Lipa$^{fl/fl}$ mice strains will be used (on C57BL/6 background). These Cre-promoters have been selected to conditionally delete *Lipa* gene in immature osteoblast-progenitors and late-stage osteoblasts/osteocytes, respectively.

Preliminary data from Dr. Rendina-Ruedy's laboratory showed high levels of CE in isolated BM-Ads. Due to the generally limited activity of cytosolic lipases in BM-AT, this tissue likely does not release free fatty acids from TGs stored in lipid droplets but rather catabolizes CE. Whether lysosomal degradation of TG and/or CE by LAL is involved in fatty acid and unesterified cholesterol release from BM-AT is currently unknown. We hope to deepen our knowledge of the specific role of this enzyme in BM-Ad metabolism by generation and description of BM-Ad specific *Lipa* knockout mouse model. Our current focus is lysosomal lipid degradation in osteoblast-lineage cells and the ongoing research keeps the role of LAL in osteoclast-mediated bone resorption out of spotlight. Although osteoclasts are clearly dependent on lysosomal function, future research will focus on the non-cell autonomous impact of LAL on bone resorption. Finally, the recently revealed role of LAL in TAG absorption via CD36 (65) suggests that there may be additional ways by which LAL affects osteoblast activity.

6. Acknowledgements

This work was supported by the National Institute of Health (NIH) National Institute of Arthritis and Musculoskeletal and Skin Diseases (NIAMS) Grants AR072123 and AR080387; and National Institute on Aging (NIA) Grant AG069795 (to E.R.R), the Austrian Science Fund FWF (W1226 Metabolic and Cardiovascular Disease (DK-MCD), F73 SFB Lipid Hydrolysis), the Province of Styria, the City of Graz, the PhD program "Molecular Medicine" of the Medical University of Graz (all to D.K.), and the Austrian Marshall Plan Foundation Fellowship. We thank the international PhD program DK-MCD for the opportunity to conduct a research stay abroad at Vanderbilt University Medical Center.

7. References

1. Rajan VR, Mitch WE. Muscle wasting in chronic kidney disease: The role of the ubiquitin proteasome system and its clinical impact. Pediatric Nephrology. 2008;23(4):527–35.
2. Osborne JC, Brewer HB. The Plasma Lipoproteins. In 1977. p. 253–337.
3. Cerqueira NMFSA, Oliveira EF, Gesto DS, Santos-Martins D, Moreira C, Moorthy HN, et al. Cholesterol Biosynthesis: A Mechanistic Overview. Biochemistry [Internet]. 2016 Oct 4;55(39):5483–506. Available from: https://pubs.acs.org/doi/10.1021/acs.biochem.6b00342
4. Li F, Zhang H. Lysosomal Acid Lipase in Lipid Metabolism and beyond. Arterioscler Thromb Vasc Biol. 2019;39(5):850–6.
5. Li F, Zhao X, Li H, Liu Y, Zhang Y, Huang X, et al. Hepatic lysosomal acid lipase drives the autophagy-lysosomal response and alleviates cholesterol metabolic disorder in ApoE deficient mice. Biochim Biophys Acta Mol Cell Biol Lipids. 2021 Dec;1866(12):159027.
6. Niemeier A, Niedzielska D, Secer R, Schilling A, Merkel M, Enrich C, et al. Uptake of postprandial lipoproteins into bone in vivo: Impact on osteoblast function. Bone. 2008;43(2):230–7.
7. Parhami F, Mody N, Gharavi N, Ballard AJ, Tintut Y, Demer LL. Role of the Cholesterol Biosynthetic Pathway in Osteoblastic Differentiation of Marrow Stromal Cells. Journal of Bone and Mineral Research. 2002 Nov 1;17(11):1997–2003.
8. Li H, Guo H, Li H. Cholesterol loading affects osteoblastic differentiation in mouse mesenchymal stem cells. Steroids. 2013 Apr;78(4):426–33.
9. You L, Sheng ZY, Tang CL, Chen L, Pan L, Chen JY. High cholesterol diet increases osteoporosis risk via inhibiting bone formation in rats. Acta Pharmacol Sin. 2011 Dec;32(12):1498–504.
10. Parhami F, Jackson SM, Tintut Y, Le V, Balucan JP, Territo M, et al. Atherogenic Diet and Minimally Oxidized Low Density Lipoprotein Inhibit Osteogenic and Promote Adipogenic Differentiation of Marrow Stromal Cells. Journal of Bone and Mineral Research. 1999 Dec 1;14(12):2067–78.
11. Pelton K, Krieder J, Joiner D, Freeman MR, Goldstein SA, Solomon KR. Hypercholesterolemia promotes an osteoporotic phenotype. American Journal of Pathology. 2012 Sep;181(3):928–36.
12. Demigné C, Bloch-Faure M, Picard N, Sabboh H, Besson C, Rémésy C, et al. Mice chronically fed a westernized experimental diet as a model of obesity, metabolic syndrome and osteoporosis. Eur J Nutr. 2006 Aug;45(5):298–306.
13. Parhami F, Tintut Y, Beamer WG, Gharavi N, Goodman W, Demer LL. Atherogenic High-Fat Diet Reduces Bone Mineralization in Mice. Journal of Bone and Mineral Research. 2001 Jan 1;16(1):182–8.

14. Chen X, Wang C, Zhang K, Xie Y, Ji X, Huang H, et al. Reduced femoral bone mass in both diet-induced and genetic hyperlipidemia mice. Bone. 2016 Dec;93:104–12.

15. Majima T, Shimatsu A, Komatsu Y, Satoh N, Fukao A, Ninomiya K, et al. Short-term Effects of Pitavastatin on Biochemical Markers of Bone Turnover in Patients with Hypercholesterolemia. Internal Medicine. 2007;46(24):1967–74.

16. MAJIMA T, KOMATSU Y, FUKAO A, NINOMIYA K, MATSUMURA T, NAKAO K. Short-term Effects of Atorvastatin on Bone Turnover in Male Patients with Hypercholesterolemia. Endocr J. 2007;54(1):145–51.

17. Yerges-Armstrong LM, Shen H, Ryan KA, Streeten EA, Shuldiner AR, Mitchell BD. Decreased Bone Mineral Density in Subjects Carrying Familial Defective Apolipoprotein B-100. J Clin Endocrinol Metab. 2013 Dec;98(12):E1999–2005.

18. Mundy G, Garrett R, Harris S, Chan J, Chen D, Rossini G, et al. Stimulation of Bone Formation in Vitro and in Rodents by Statins. Science (1979). 1999 Dec 3;286(5446):1946–9.

19. Mandal CC. High cholesterol deteriorates bone health: New insights into molecular mechanisms. Vol. 6, Frontiers in Endocrinology. Frontiers Media S.A.; 2015.

20. Ghosh-Choudhury N, Mandal CC, Choudhury GG. Statin-induced Ras activation integrates the phosphatidylinositol 3-kinase signal to Akt and MAPK for bone morphogenetic protein-2 expression in osteoblast differentiation. Journal of Biological Chemistry. 2007 Feb 16;282(7):4983–93.

21. Liu S, Bertl K, Sun H, Liu ZH, Andrukhov O, Rausch-Fan X. Effect of simvastatin on the osteogenetic behavior of alveolar osteoblasts and periodontal ligament cells. Hum Cell. 2012 Jun;25(2):29–35.

22. Maeda T, Matsunuma A, Kurahashi I, Yanagawa T, Yoshida H, Horiuchi N. Induction of osteoblast differentiation indices by statins in MC3T3-E1 cells. J Cell Biochem. 2004;92(3):458–71.

23. Korbelius M, Kuentzel KB, Bradić I, Vujić N, Kratky D. Recent insights into lysosomal acid lipase deficiency. Trends in Molecular Medicine. Elsevier Ltd; 2023.

24. A. ABRAMOV, M.D. S. SCHORR, M.D. and M. WOLMAN MD. GENERALIZED XANTHOMATOSIS WITH CALCIFIED ADRENALS. AMA J Dis Child. 1956;

25. Boldrini R, Devito R, Biselli R, Filocamo M, Bosman C. Wolman disease and cholesteryl ester storage disease diagnosed by histological and ultrastructural examination of intestinal and liver biopsy. Pathol Res Pract. 2004;200(3):231–40.

26. Pericleous M, Kelly C, Wang T, Livingstone C, Ala A. Wolman's disease and cholesteryl ester storage disorder: the phenotypic spectrum of lysosomal acid lipase deficiency. Lancet Gastroenterol Hepatol. 2017 Sep;2(9):670–9.

27. Sloan HR, Fredrickson DS. Enzyme deficiency in cholesteryl ester storage disease. Journal of Clinical Investigation [Internet]. 1972 Jul 1;51(7):1923–6. Available from: http://www.jci.org/articles/view/106997

28. Du H, Heur M, Duanmu M, Grabowski GA, Hui DY, Witte DP, et al. Lysosomal acid lipase-deficient mice: Depletion of white and brown fat, severe hepatosplenomegaly, and shortened life span. J Lipid Res. 2001;42(4):489–500.

29. Dubland JA, Francis GA. Lysosomal acid lipase: At the crossroads of normal and atherogenic cholesterol metabolism. Front Cell Dev Biol. 2015;3(FEB):1–11.

30. Schlager S, Vujic N, Korbelius M, Duta-Mare M, Dorow J, Leopold C, et al. Lysosomal lipid hydrolysis provides substrates for lipid mediator synthesis in murine macrophages. Oncotarget. 2017;8(25):40037–51.

31. Radović B, Vujić N, Leopold C, Schlager S, Goeritzer M, Patankar J V., et al. Lysosomal acid lipase regulates VLDL synthesis and insulin sensitivity in mice. Diabetologia. 2016;59(8):1743–52.

32. Bianco V, Korbelius M, Vujic N, Akhmetshina A, Amor M, Kolb D, et al. Impact of (intestinal) LAL deficiency on lipid metabolism and macrophage infiltration. Mol Metab [Internet]. 2023 Jul;73:101737. Available from: https://linkinghub.elsevier.com/retrieve/pii/S2212877823000716

33. Helderman RC, Whitney DG, Duta-Mare M, Akhmetshina A, Vujic N, Jayapalan S, et al. Loss of function of lysosomal acid lipase (LAL) profoundly impacts osteoblastogenesis and increases fracture risk in humans. Bone. 2021 Jul 1;148.

34. Attané C, Estève D, Chaoui K, Iacovoni JS, Corre J, Moutahir M, et al. Human Bone Marrow Is Comprised of Adipocytes with Specific Lipid Metabolism. Cell Rep. 2020;30(4):949-958.e6.

35. Justesen J, Stenderup K, Ebbesen EN, Mosekilde L, Steiniche T, Kassem M. Adipocyte tissue volume in bone marrow is increased with aging and in patients with osteoporosis. Biogerontology. 2001;2(3):165–71.

36. Scheller EL, Doucette CR, Learman BS, Cawthorn WP, Khandaker S, Schell B, et al. Region-specific variation in the properties of skeletal adipocytes reveals regulated and constitutive marrow adipose tissues. Nat Commun. 2015 Nov 24;6(1):7808.

37. Bredella MA, Torriani M, Ghomi RH, Thomas BJ, Brick DJ, Gerweck A V., et al. Vertebral Bone Marrow Fat Is Positively Associated With Visceral Fat and Inversely Associated With IGF-1 in Obese Women. Obesity. 2011 Jan;19(1):49–53.

38. Doucette CR, Horowitz MC, Berry R, MacDougald OA, Anunciado-Koza R, Koza RA, et al. A High Fat Diet Increases Bone Marrow Adipose Tissue (MAT) But Does Not Alter Trabecular or Cortical Bone Mass in C57BL/6J Mice. J Cell Physiol. 2015 Sep;230(9):2032–7.

39. Luu W, Sharpe LJ, Gelissen IC, Brown AJ. The role of signalling in cellular cholesterol homeostasis. IUBMB Life. 2013 Aug;65(8):675–84.

40. Zampelas A, Magriplis E. New Insights into Cholesterol Functions: A Friend or an Enemy? Vol. 11, Nutrients. MDPI AG; 2019.

41. DeMambro VE, Clemmons DR, Horton LG, Bouxsein ML, Wood TL, Beamer WG, et al. Gender-Specific Changes in Bone Turnover and Skeletal Architecture in Igfbp-2-Null Mice. Endocrinology. 2008 May 1;149(5):2051–61.

42. Bligh EG, Dyer WJ. A RAPID METHOD OF TOTAL LIPID EXTRACTION AND PURIFICATION. Can J Biochem Physiol. 1959 Aug 1;37(8):911–7.

43. Maridas DE, Rendina-Ruedy E, Le PT, Rosen CJ. Isolation, Culture, and Differentiation of Bone Marrow Stromal Cells and Osteoclast Progenitors from Mice. Journal of Visualized Experiments. 2018 Jan 6;(131).

44. Bradić I, Kuentzel KB, Honeder S, Grabner GF, Vujić N, Zimmermann R, et al. Off-target effects of the lysosomal acid lipase inhibitors Lalistat-1 and Lalistat-2 on neutral lipid hydrolases. Mol Metab. 2022 Jul;61(April):101510.

45. Kim H, Kim M, Im SK, Fang S. Mouse Cre-LoxP system: general principles to determine tissue-specific roles of target genes. Lab Anim Res. 2018;34(4):147.

46. Hauschka P V., Lian JB, Cole DE, Gundberg CM. Osteocalcin and matrix Gla protein: vitamin K-dependent proteins in bone. Physiol Rev. 1989 Jul 1;69(3):990–1047.

47. Bowden KL, Bilbey NJ, Bilawchuk LM, Boadu E, Sidhu R, Ory DS, et al. Lysosomal Acid Lipase Deficiency Impairs Regulation of ABCA1 Gene and Formation of High Density Lipoproteins in Cholesteryl Ester Storage Disease. Journal of Biological Chemistry [Internet]. 2011 Sep;286(35):30624–35. Available from: https://linkinghub.elsevier.com/retrieve/pii/S0021925820723458

48. Du H, Schiavi S, Levine M, Mishra J, Heur M, Grabowski GA. Enzyme therapy for lysosomal acid lipase deficiency in the mouse. Hum Mol Genet. 2001;10(16):1639–48.

49. Bernstein DL, Hülkova H, Bialer MG, Desnick RJ. Cholesteryl ester storage disease: Review of the findings in 135 reported patients with an underdiagnosed disease. J Hepatol [Internet]. 2013;58(6):1230–43. Available from: http://dx.doi.org/10.1016/j.jhep.2013.02.014

50. Couasnay G, Madel M, Lim J, Lee B, Elefteriou F. Sites of Cre-recombinase activity in mouse lines targeting skeletal cells. Journal of Bone and Mineral Research. 2021 Sep 22;36(9):1661–79.

51. Scheller EL, Leinninger GM, Hankenson KD, Myers Jr, MG, Krebsbach PH. Ectopic Expression of Col2.3 and Col3.6 Promoters in the Brain and Association with Leptin Signaling. Cells Tissues Organs. 2011;194(2–4):268–73.

52. Park JS, Baek WY, Kim YH, Kim JE. In vivo expression of Osterix in mature granule cells of adult mouse olfactory bulb. Biochem Biophys Res Commun. 2011 Apr;407(4):842–7.

53. Frenkel B, Capparelli C, van Auken M, Baran D, Bryan J, Stein JL, et al. Activity of the Osteocalcin Promoter in Skeletal Sites of Transgenic Mice and during Osteoblast Differentiation in Bone Marrow-Derived Stromal Cell Cultures: Effects of Age and Sex*. Endocrinology. 1997 May 1;138(5):2109–16.

54. Quarles LD, Siddhanti SR, Medda S. Developmental regulation of osteocalcin expression in MC3T3-E1 osteoblasts: Minimal role of the proximal E-box cis-acting promoter elements. J Cell Biochem. 1997 Apr;65(1):11–24.

55. Elefteriou F, Yang X. Genetic mouse models for bone studies—Strengths and limitations. Bone. 2011 Dec;49(6):1242–54.

56. Zhang M, Xuan S, Bouxsein ML, von Stechow D, Akeno N, Faugere MC, et al. Osteoblast-specific Knockout of the Insulin-like Growth Factor (IGF) Receptor Gene Reveals an Essential Role of IGF Signaling in Bone Matrix Mineralization. Journal of Biological Chemistry. 2002 Nov;277(46):44005–12.

57. Tan X, Weng T, Zhang J, Wang J, Li W, Wan H, et al. Smad4 is required for maintaining normal murine postnatal bone homeostasis. J Cell Sci. 2007 Jul 1;120(13):2162–70.

58. Sando GN, Rosenbaum LM. Human lysosomal acid lipase/cholesteryl ester hydrolase. Purification and properties of the form secreted by fibroblasts in microcarrier culture. Journal of Biological Chemistry. 1985 Dec;260(28):15186–93.

59. Sando GN, Ma GP, Lindsley KA, Wei YP. Intercellular transport of lysosomal acid lipase mediates lipoprotein cholesteryl ester metabolism in a human vascular endothelial cell-fibroblast coculture system. Cell Regul. 1990 Aug;1(9):661–74.

60. Sando GN, Henke VL. Recognition and receptor-mediated endocytosis of the lysosomal acid lipase secreted by cultured human fibroblasts. J Lipid Res. 1982 Jan;23(1):114–23.

61. Scheller EL, Khandaker S, Learman BS, Cawthorn WP, Anderson LM, Pham HA, et al. Bone marrow adipocytes resist lipolysis and remodeling in response to β-adrenergic stimulation. Bone. 2019 Jan;118:32–41.

62. Takahashi Y, Shinoda A, Kamada H, Shimizu M, Inoue J, Sato R. Perilipin2 plays a positive role in adipocytes during lipolysis by escaping proteasomal degradation. Sci Rep. 2016 Feb 15;6(1):20975.

63. Sun C, Mao S, Chen S, Zhang W, Liu C. PPARs-Orchestrated Metabolic Homeostasis in the Adipose Tissue. Int J Mol Sci. 2021 Aug 20;22(16):8974.

64. de Paula FJA, Rosen CJ. Marrow Adipocytes: Origin, Structure, and Function. Annu Rev Physiol. 2020 Feb 10;82(1):461–84.

65. Fischer AW, Jaeckstein MY, Gottschling K, Heine M, Sass F, Mangels N, et al. Lysosomal lipoprotein processing in endothelial cells stimulates adipose tissue thermogenic adaptation. Cell Metab. 2021 Mar;33(3):547-564.e7.